Chemical Geology
March 2023, Volume 620, Pages 121326 (14p.)
https://doi.org/10.1016/j.chemgeo.2023.121326
https://archimer.ifremer.fr/doc/00817/92849/

Viscosity of crystal-free silicate melts from the active submarine volcanic chain of Mayotte

Verdurme Pauline [1], Le Losq Charles [2], Chevrel Oryaëlle [1, 2, 3], Pannefieu Salomé [2], Médard Etienne [1], Berthod Carole [1, 2, 4], Komorowski Jean-Christophe [2], Bachèlery Patrick [1], Neuville Daniel R. [2], Gurioli Lucia [1]

[1] Université Clermont Auvergne, CNRS, IRD, OPGC, Laboratoire Magmas et Volcans, F-63000 Clermont-Ferrand, France
[2] Université Paris Cité, Institut de physique du globe de Paris, CNRS, F-75005 Paris, France
[3] Observatoire volcanologique du Piton de la Fournaise, Institut de physique du globe de Paris, 97418 La Plaine des Cafres, France
[4] Observatoire volcanologique et sismologique de la Guadeloupe, Institut de physique du globe de Paris, 97113 Gourbeyre, France

Abstract :

Following an unprecedented seismic activity that started in May 2018, a new volcanic edifice, now called Fani Maoré, was constructed on the ocean floor 50 km east of the island of Mayotte (Indian Ocean). This volcano is the latest addition to a volcanic chain characterized by an alkaline basanite-to-phonolite magmatic differentiation trend. Here, we performed viscosity measurements on five silicate melts representative of the East-Mayotte Volcanic Chain compositional trend: two basanites from Fani Maoré, one tephriphonolite and two phonolites from different parts of the volcanic chain. A concentric cylinder viscometer was employed at super-liquidus conditions between 1500 K and 1855 K and a creep apparatus was used for measuring the viscosity of the undercooled melts close to the glass transition temperature in the air. At super-liquidus temperatures, basanites have the lowest viscosity (0.11–0.34 to 0.99–1.16 log10 Pa·s), phonolites the highest (1.75–1.91 to 3.10–3.89 log10 Pa·s), while the viscosity of the tephriphonolite falls in between (0.89–1.97 log10 Pa·s). Near the glass transition, viscosity measurements have only been performed for one phonolite melt because obtaining pure glass samples for the basanite and tephriphonolite compositions was unsuccessful. This was due to the formation of nanolites upon quench as evidenced by Raman spectroscopy. The phonolite viscosity ranges from of 10.19 log10 Pa·s at 1058 K to 12.30 log10 Pa·s at 986 K. Comparison with existing empirical models revealed an underestimation of 1.2 to 2.0 log units at super-liquidus and undercooled temperatures, respectively, for the phonolite. This emphasizes (i) the lack of data falling along the alkaline basanite-to-phonolite magmatic differentiation trend to calibrate empirical models, and (ii) the complexity of modeling viscosity variations as a function of temperature and chemical composition for alkaline compositions. The new measurements indicate that, at eruptive temperatures between 1050 °C and 1150 °C (1323–1423 K), the oxidized, anhydrous, crystal-free and bubble-free basanite melt is very fluid, presenting a viscosity around 2.6 log10 Pa·s. In contrast, the anhydrous phonolite crystal- and bubble-free melt would have a viscosity around 6–10 log10 Pa·s at expected eruptive temperatures, which range from 800 to 1000 °C (1073–1273 K). Considering that both basanite and phonolite lavas from the Mayotte submarine volcanic chain

contain <6% crystals and a significant amount of water, such viscosity values are probably upper limits. The new viscosity measurements are essential to define eruptive models and to better understand the storage and transport dynamics of Comoros Archipelago magmas, and of alkaline magmas in general, from the source to the surface.

Keywords : rheology, alkali magmas, submarine volcano, volcanic eruption, Raman spectroscopy

1. Introduction

Following an unprecedented intense seismic crisis that started in May 2018 (Lemoine et al. 2020; Feuillet et al. 2021), oceanographic surveys revealed a new submarine volcanic edifice, named Fani Maoré, 936 m tall with a base at around 3,500 m depth situated 50 km east of Mayotte (Indian Ocean). This large eruption has extruded around 6.55 km^3 of basanite magma, with first estimates of magma transfer rates from source to surface of a minimum of 30 days (Cesca et al. 2020; Berthod et al. 2021a). The source of this magma is evaluated to be located at 30 - 50 km depth into the underlying mantle, with the potential involvement of an intermediate magma chamber at ~17 km depth (Berthod et al. 2021b). This new volcano is an addition to the East-Mayotte Volcanic Chain characterized by the emission of magmas falling along an alkaline basanite-to-phonolite magmatic differentiation trend. This volcanic chain is quite complex and characterized by large effusive lava flow fields, and by the presence of more explosive volcanoes (**Figure 1**) (Puzenat et al. 2023; Gurioli et al. 2023; Komorowski et al. 2023). To better understand and constrain the storage processes and transfer rates of the magmas that feed the East-Mayotte Volcanic Chain as well as the dynamics of their emplacement at surface, it is necessary to constrain the viscosity of the basanite-to-phonolite melts because it determines the mobility of magmas toward surface as well as their fragmentation behavior in the conduit and their flow on the surface (Dingwell et al. 1996; Papale 1999; Pistolesi et al. 2011).

To constrain the viscosity of magmas and lavas, one can potentially rely on the various experimental and modeling efforts that led to important improvements in our knowledge of how it is controlled by temperature (Vogel 1921; Tamman and Hesse 1926; Fulcher 1925; Adam and Gibbs 1965; Nascimento and Aparicio 2007), chemical composition (Bottinga and Weill 1972; Shaw 1972; Giordano et al. 2008), volatile elements (e.g.,Whittington et al.

2000, 2001), bubbles (Lejeune et al. 1999; Llewellin and Manga et al. 2005) and crystal contents (Lejeune and Richet 1995; Kolzenburg et al. 2022) as well as nonequilibrium crystallization processes (Di Fiore et al. 2022; Kolzenburg et al. 2022, 2018; Vetere et al. 2019). Yet, there is not a general and very accurate viscosity model to date, due to the complexity in estimating the individual influence and global interplay of the different parameters listed above. Focusing only on the silicate melt phase of magmas and lavas, many effects exist at the atomic level, such as aluminum coordination changes or metal cation mixing, that result in strong and non-linear variations in melt viscosity depending on composition. In particular, in alkali-rich melts, the way Na and K mix may strongly affect viscosity (Poole, 1948; Richet, 1984; Le Losq and Neuville, 2013, 2017). In Al-poor melts, the ideal mixing between Na and K results in an important decrease in viscosity (Richet 1984), whereas in Al-rich melts, Na and K occupy different environments and do not mix ideally (Le Losq and Neuville 2013; Le Losq et al., 2017, 2021b). At given temperature, this leads to increasing viscosity by several orders of magnitude upon increasing K/(K+Na) ratio in the melt. Existing parametric viscosity models (e.g., Hui and Zhang 2007; Giordano et al. 2008) failed to properly reproduce such an effect (Le Losq and Neuville 2013; Robert et al. 2019). Therefore, their accuracy for the prediction of the viscosity of melts along alkaline magmatic series is to be improved. Only models integrating thermodynamic and physico-chemical knowledge allow properly modeling the way Na and K non-ideal mixing alters the viscosity of Al-rich alkali melts. However, this has been applied only on quaternary alkali aluminosilicate melts far from natural compositions (Robert et al. 2019; Starodub et al. 2019; Le Losq et al. 2021b). Therefore, to properly constrain the viscosity of alkali melts, one needs to use *ad hoc* models for increased precision, as it has been performed for the phonolite of Erebus volcano (Antarctica) for instance (Le Losq et al. 2015a).

In this contribution, we present new viscosity measurements performed on samples representative of the magma compositions that can be found along the East-Mayotte submarine volcanic chain. Those samples fall along the moderately silica-undersaturated trend ("Karthala-trend") of the Comoros Archipelago (Pelleter et al. 2014; Bachèlery et al. 2016; Bachèlery and Hémond 2016). The studied compositions include two basanite lavas from the recent eruption (Fani Maoré volcano), and two phonolite and a tephriphonolite samples from other emission sites in the submarine volcanic chain (Berthod et al. 2021a; Feuillet et al. 2021; Puzenat et al. 2023; **Figure 1**). Viscosity is measured with a concentric cylinder viscometer at super-liquidus temperatures, in the 10^{0} - 10^{6} Pa·s range, and with a creep apparatus close to the glass transition temperature between 10^{8} and 10^{13} Pa·s in the air. We also examine the effect of water content on melt viscosity for the different magma compositions present at Mayotte. The results (i) provide the foundation necessary to investigate the eruptive behavior of the Mayotte volcanic system, (ii) strengthen the current knowledge on alkaline series and (iii) could contribute to refine the pre-existing empirical viscosity models based on chemical composition.

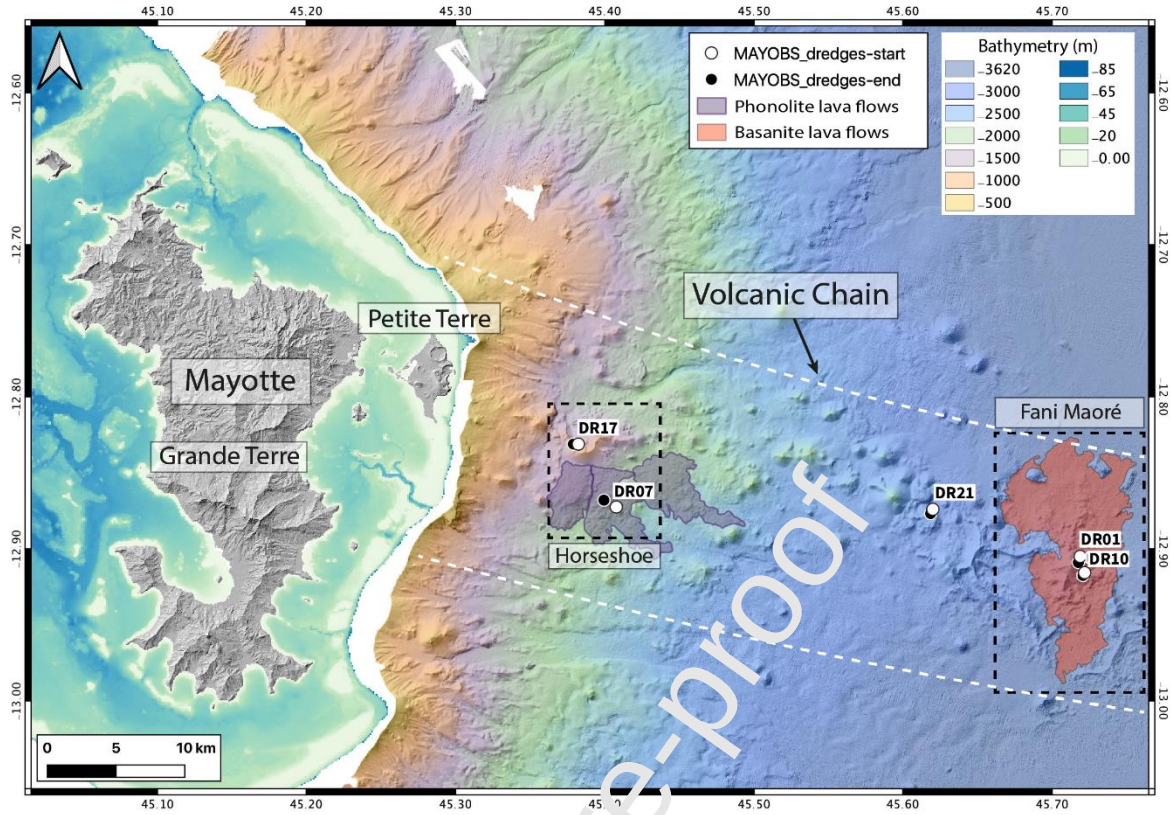

Figure 1. *Geological map of the submarine volcanic chain of Mayotte showing the location of the dredged samples (DR labels). Fani Maoré outline is modified from Feuillet et al. (2021). Modified from Berthod et al. (2021a). Background is the bathymetry from the Homonim project (SHOM 2015). DEM Litto3D IGN-SHOM (SHOM 2016) and MAYOBS1 (doi:10.17600/18001217).*

2. Materials and Methods

2.1. *Starting material*

In this study, the investigated samples were collected by dredging operations (Berthod et al. 2022) that collected between 100 - 1000 kg of rocks, from water depths ranging from 1,370 to 3,455 m (**Figure 1**). These dredges were operated by the R/V *Marion Dufresne II* and R/V *Pourquoi Pas?* during the following oceanographic cruises (Rinnert et al. 2019): MAYOBS 1 (Feuillet 2019), MAYOBS 2 (Jorry,2019), MAYOBS 4 (Fouquet and Feuillet 2019), MAYOBS 15 (Rinnert et al. 2020), and GEOFLAMME (Rinnert et al. 2021) (**Table 1**).

Table 1. *Location of the dredges performed during the oceanographic cruises. Latitudes and Longitudes are given in decimal degrees (DD).*

Dredges	Oceanographic cruises	DOI of the oceanographic cruises 10.18142/291	Start dredging			End dredging		
			Latitude	*Longitude*	*Depth*	*Latitude*	*Longitude*	*Depth*
DR01	MAYOBS 1	10.17600/18001217	-12.905	45.719	3050 m	-12.909	45.718	2820 m
DR07	MAYOBS 2	10.17600/18001222	-12.872	45.4[illegible]	1590 m	-12.868	45.399	1585 m
DR10	MAYOBS 4	10.17600/18001238	-12.91[illegible]	45.722	3120 m	-12.918	45.721	2950 m
DR17	MAYOBS 15	10.17600/18001745	-12.83[illegible]	45.382	1370 m	-12.831	45.379	1340 m
DR21	GEOFLAMME	10.17600/1800129[illegible]	-12.874	45.620	2719 m	-12.876	45.618	2629 m

We selected five samples that represent the diverse composition of the volcanic deposits along the Mayotte submarine volcanic chain (**Fig. 1** and **Table 2**). Two samples (MAY01-DR010101 and MAY04-DR[illegible]0504, hereafter named DR01 and DR10, respectively) are from Fani Maoré, the new volcano that has been in activity from 2018 to 2021 (**Fig. 1**, Lemoine et al. 2020; Berthod et al. 2021b; Feuillet et al. 2021). These two samples are fragments of basanite lava flows collected on the central edifice and were emitted during the first year of the eruption (before May 2019, Berthod et al. 2021b). Two other samples (MAY02-DR070201 and MAY15-DR170404, hereafter named DR07 and DR17, respectively) were recovered at 10 - 15 km east of Petite Terre Island of Mayotte on the "Horseshoe" volcanic structure (**Fig. 1**, Berthod et al. 2021a; Feuillet et al. 2021; Puzenat et al. 2023; Gurioli et al. 2023). DR07 is a fragment of a Holocene phonolite lava flow located on the southeastern part of the Horseshoe site. DR17 is a phonolite pyroclast bomb collected

at the bottom of the internal western side slope of the Horseshoe structure. Finally, the fifth sample (GFL-DR2110, hereafter named DR21) was collected on a seamount located in the middle of the submarine volcanic chain, 10 km west of Fani Maoré (Rinnert et al. 2021). This sample is a fragment of lava and has a tephriphonolite composition.

About 200 g of each sample were used to produce the starting glasses necessary for the experiments. The rock samples were first crushed and powdered. A small portion of the powder was used for bulk rock chemical analyses and the rest was used for viscosity measurements. Chemical analyses have also been performed on glass chips retrieved after high- and low-temperatures viscometry.

2.2. Major element analyses

Bulk rock major element composition of the starting materials was analyzed at Laboratoire Magmas et Volcans (LMV, Clermont-Ferrand, France). Samples were crushed into millimeter-size chips using homemade thermally hardened steel jaws, and powdered in a motorized agate mortar. Major elements were analyzed by Inductively Coupled Plasma Atomic Emission Spectrometry (ICP-AES). Powdered samples were melted with $LiBO_2$ in a magnetic induction oven at 1100 °C for 5 min using graphite crucibles. The glass beads were then dissolved in a solution of deionized water and nitric acid (1 M) and diluted by a factor of 2000 to produce the solution analyzed by an Agilent 5800 VDV ICP AES in radial mode. Analytical uncertainties (± 2σ) vary between 1 and 3 % except for K_2O, MnO (4 %) and P_2O_5 (7 %) for the DR-N standard (diorite). For the analysis, the plasma flow was 12 L/min, the nebulizer flow was 0.7 L/min and the radio frequency power was 1.2 kW.

Glass chips resulting from spindle quench after the super-liquidus viscometry were mounted as polished sections for chemical analysis. Those were carried out using the CAMECA SX Five Tactis electron microprobe at LMV. We used an accelerating potential of 15 kV at current of 8 nA, with a defocused beam of 20 μm diameter to avoid Na migration under the

electron beam. Natural and synthetic mineral standards, including orthoclase (K, Al), albite (Na), wollastonite (Si, Ca), fayalite (Fe), forsterite (Mg), $TiMnO_3$ (Ti, Mn), NiO (Ni), Cr_2O_3 (Cr), and fluorapatite (P) were used for routine calibration. The resulting post-experiment compositions are an average of at least ten measurements made on glass.

We calculated the NBO/T parameter (number of non-bridging oxygen per tetrahedral), representing the degree of polymerization of the melt following Mysen et al. (1982):

$$\frac{NBO}{T} = \frac{(2O)-(4T)}{T}, \quad (1)$$

with O the atomic proportion of oxygen atoms and T that of cations entering as network formers in tetrahedral coordination, namely SiO_2, TiO_2, Al_2O_3, and Fe_2O_3 (see for a review of such concepts Le Losq et al. 2019). Here, the total iron is expressed as Fe^{3+} as the viscosity experiments were performed in an oxidizing environment. This assumption is a valid simplification: estimations with the Moretti (2005) model yields 90 % or more of Fe residing in the melt as Fe_2O_3 at the conditions of our experiments. The NBO/T of the natural melt may thus be higher, considering the occurrence of reduced iron and its influence on the melt structure (e.g., Le Losq et al. 2021a).

2.3. High temperature viscometry

High temperature viscosity measurements are performed at super-liquidus conditions in air, using a concentric cylinder viscometer (Dingwell 1986; Spera et al. 1988) at the Institut de physique du globe de Paris (IPGP, Paris, France). Powdered glass samples are first melted at 1800 K in a $Pt_{95}Au_5$ cylindrical crucible (50 mm height, 27 mm inner diameter, 1 mm wall thickness) in a muffle furnace. Once the crucible is full, it is inserted in the hot zone of the viscometer vertical tube furnace, heated by Super Kanthal 33 elements in air. Sample temperature is recorded using Pt_6Rh_{30} type B thermocouple in contact with the bottom of the

crucible. The temperature gradient inside the crucible was initially checked by measuring temperature at different depths inside the crucible. The vertical and radial temperature gradients in the crucible are respectively lower than 2 K across 5 cm and 1 K across 2.7 cm at 1500 K and even lower at 1800 K. As a result, errors on reported sample temperatures for those experiments are of 2 K at most. The inner rotating spindle size is 14 mm in diameter, 21 mm in height and has 23° conical extremities to reduce termination effects and a 5 mm diameter stem. Viscosity is measured using a Rheomat 115 rheometer head, which allows rotating the cylinder at angular velocities ranging between 0.01 and 81.68 rad s^{-1} rpm. In practice, we used angular velocities between 10^{-2} and 10^{1} rad s^{-1}. Overall, this corresponds to shear rates during experiments that range from 1.10^{-4} to 21 s^{-1}. Effective torque can reach 50 mNm, but in practice, we never exceeded 2/3 of this maximal value. At each temperature, we measure the apparent torque at different rotational speeds, to check for the apparition of non-Newtonian effects. None were detected during the present experiments. The apparent torque is then converted in viscosity, via a calibration made using the reference glass sample NBS SRM 710a, for which the viscosity-temperature relationship is accurately known and provided by the National Bureau of Standards. The accuracy is of the order of 0.02 $\log_{10}$ Pa·s (e.g., Neuville 2006).

2.4. Low temperature viscometry

Low temperature viscosity measurements are performed near the glass transition temperature (T_g) using a creep apparatus at IPGP (Neuville and Richet 1991; Neuville 2006). Glass samples used for measurements are (i) a parallelepiped of 7.9 mm length, and (ii) a small cylinder of 2.2 mm diameter x 8.1 mm length. A silver cylinder is placed around the sample, creating a small chamber in which temperature is homogeneous. Lateral and vertical temperature gradients are controlled using two Pt-$PtRh_{10}$ thermocouples (ITS90 type S thermocouples); before and during each measurement, lateral and vertical temperature

gradients were always lower than 0.2 K. To measure sample viscosity at a given temperature, we performed 20 to 30 measurements at different stresses (between 6.4 and 8.2 log Nm^{-2}) to check for the occurrence of a non-Newtonian behavior, which could be a sign of crystallization of the sample. Each reported viscosity value at a given temperature is the statistical mean of these measurements. Measurements carried out on the NBS 717 glass show that errors on viscosity measurements are lower than 0.03 $\log_{10}$ Pa·s with this apparatus (e.g., Neuville 2006).

2.5. ***Raman spectroscopy***

The Raman spectra of the glasses (pre- and post-experiments) were recorded with the Labram HR Evolution spectrometer available at IPGP, equipped with a Peltier-cooled CCD and a 1800 lines mm^{-1} grating. The samples were excited with a Coherent MX 488 nm solid-state laser focused through a ×50 Olympus objective on the sample surface. The confocal aperture of the spectrometer was set to 50. With this setup, spectral resolution is ~3 cm^{-1} and spatial resolution is ≤1 μm^{-1}. All spectra were recorded with the laser focused at 3-5 µm below the sample's surface to avoid any surface effects (Behrens et al. 2006; Schiavi et al. 2018). The laser power on the sample has been adjusted to lower than 10 mW to avoid any potential damage on the sample (iron oxidation effects or melting). Potential damage was checked by recording several spectra on the same spot and varying laser power, without the identification of any effect. Raman data treatment was performed using the Python programming software, with the *rampy* open-source software library (Le Losq 2018).

3. Results

3.1. Major element composition

The bulk rock chemical composition of the pre-experiment samples and the post-experiments glass compositions, determined by ICP-AES and by electron microprobe analyses respectively, are reported in **Table 2** and presented in **Figure 2**.

DR01 and DR10 basanites have a very similar composition, comprising between 47.1 and 47.7 wt% SiO_2 and 7.2 to 7.8 alkali ($Na_2O + K_2O$) wt% (**Fig. 2**). These samples have low MgO contents, between ~4.8 and ~5.4 wt%, and high $FeO_{tot.}$ contents, between ~12.5 and ~12.7 wt% (**Table 2**), making them the most iron-rich among all the studied samples from the East-Mayotte submarine volcanic chain. DR07 and DR17 phonolite samples have similar silica contents of 57.7 - 58.9 wt% SiO_2, but DR07 has an alkali content of 13.0 wt% while DR17 is richer in alkali with 14.2 wt% (**Fig. 2** and **Table 2**). Compared to basanite samples, phonolite samples have lower $FeO_{tot.}$ contents, ranging from 6.1 to 7.2 wt%. Finally, sample DR21 is tephriphonolite composition, falling in between the basanite and phonolite fields of the TAS diagram (**Fig. 2**) with SiO_2 and alkali contents of 53.2 wt% and 10.8 wt%, respectively (**Table 2**) and an intermediate $FeO_{tot.}$ content of 10 wt%.

For most samples, the major element contents show no significant differences before and after viscosity experiments expect a slight alkali loss (**Table 2**). We however note that the composition of DR17 after the high-temperature experiment has a higher SiO_2 content of 1.5 wt%. This is accompanied by iron loss of 0.5 wt% (**Table 2**).

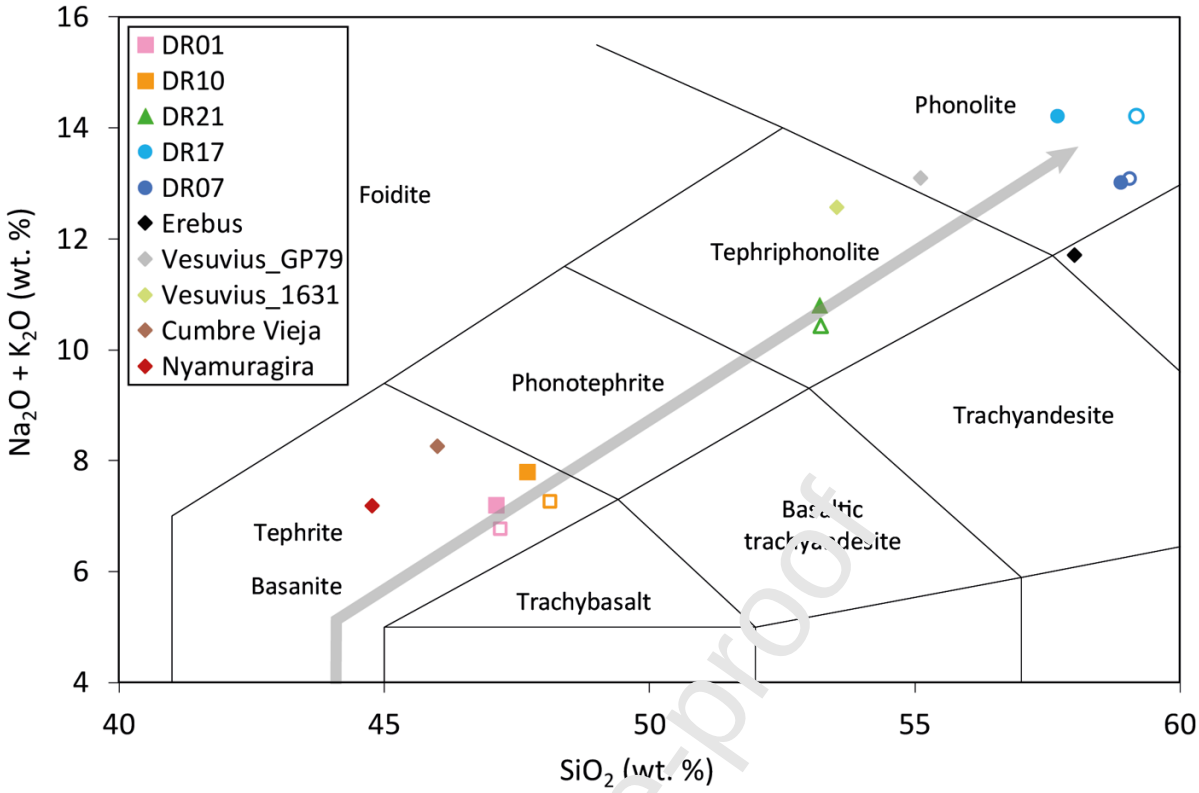

Figure 2. *TAS diagram showing normalized compositions of the studied samples before (filled symbols, ICP-AES) and after (empty symbols, Electron Microprobe) viscosity measurements. Compositions of: phonolite lavas from Erebus and Vesuvius (GP79, Grey Pumice of the 79 eruption) (data from Le Losq et al. 2015a; of basanite lavas from Cumbre Vieja (Castro and Feisel 2022), Nyamuragira (Morrison et al. 2020) and; of tephriphonolite from Vesuvius (Tephra from the 1631 eruption) (Romano et al. 2003) are also shown for comparison. The grey arrow shows the moderately silica-undersaturated trend ("Karthala-trend") identified by Pelleter et al. (2014) and Bachèlery and Hémond (2016). Error bars are smaller than symbol size.*

Table 2. *Normalized major element composition in wt% pre- (first line) and post- (second line) experiments of the studied samples. The post-experiment composition are an average of at least ten measurements made on glass. The composition of Erebus and Vesuvius GP79 (Le Losq et al. 2015a), Cumbre Vieja (Castro and Feisel 2022),* Nyamuragira *(Morrison et al. 2020) and Vesuvius 1631 (Romano et al. 2003) are also reported for comparison. 2σ errors are given in parenthesis.*

Sample	SiO_2	TiO_2	Al_2O_3	FeO(t)	MnO	MgO	CaO	Na_2O	K_2O	P_2O_5	NBO/T
Before and after experiments											
DR01	47.1 (± 0.707)	3.3 (± 0.050)	15.3 (± 0.230)	12.7 (± 0.191)	0.2 (± 0.008)	5.4 (± 0.081)	7.3 (± 0.120)	4.7 (± 0.071)	2.5 (± 0.100)	1.6 (± 0.112)	0.32
	47.2 (± 0.307)	3.4 (± 0.022)	14.8 (± 0.096)	13.2 (± 0.086)	0.3 (± 0.002)	5.4 (± 0.035)	7.3 (± 0.047)	4.4 (± 0.028)	2.4 (± 0.016)	1.6 (± 0.011)	-
DR10	47.7 (± 0.716)	3.1 (± 0.047)	15.2 (± 0.228)	12.5 (± 0.188)	0.2 (± 0.008)	4.8 (± 0.072)	6.8 (± 0.102)	5.2 (± 0.078)	2.6 (± 0.104)	1.9 (± 0.133)	0.33
	48.1 (± 0.388)	3.2 (± 0.022)	15.3 (± 0.121)	12.6 (± 0.043)	0.3 (± 0.002)	4.9 (± 0.003)	6.8 (± 0.041)	4.6 (± 0.049)	2.6 (± 0.037)	1.7 (± 0.002)	-
DR21	53.2 (± 0.798)	1.6 (± 0.024)	16.5 (± 0.248)	9.8 (± 0.147)	0.3 (± 0.012)	1.9 (± 0.029)	4.2 (± 0.063)	6.8 (± 0.102)	4.0 (± 0.160)	1.0 (± 0.070)	0.20
	53.2 (± 0.348)	1.7 (± 0.011)	16.9 (± 0.110)	10.0 (± 0.065)	0.3 (± 0.002)	2.0 (± 0.013)	4.5 (± 0.029)	6.5 (± 0.042)	4.0 (± 0.026)	1.0 (± 0.007)	-
DR07	58.9 (± 0.884)	0.4 (± 0.006)	18.2 (± 0.273)	7.2 (± 0.108)	0.3 (± 0.012)	0.4 (± 0.006)	1.6 (± 0.024)	7.6 (± 0.114)	5.4 (± 0.216)	0.3 (± 0.021)	0.10
	59.1 (± 0.386)	0.4 (± 0.022)	18.6 (± 0.121)	6.4 (± 0.042)	0.3 (± 0.002)	0.3 (± 0.003)	1.6 (± 0.010)	7.6 (± 0.048)	5.7 (± 0.037)	0.3 (± 0.002)	-
DR17	57.7 (± 0.866)	0.1 (± 0.002)	18.7 (± 0.281)	6.1 (± 0.092)	0.3 (± 0.004)	0.1 (± 0.002)	1.3 (± 0.020)	8.6 (± 0.130)	5.6 (± 0.224)	0.1 (± 0.007)	0.11
	59.2 (± 0.387)	0.1 (± 0.001)	19.1 (± 0.125)	5.6 (± 0.036)	0.2 (± 0.002)	0.1 (± 0.001)	1.3 (± 0.009)	8.4 (± 0.055)	5.8 (± 0.038)	0.1 (± 0.001)	-
Cumbre Vieja	46.1	3.8	16.6	11.4	0.2	4.0	9.4	5.8	2.5	1.3	0.37
Nyamuragira	46.0	3.8	17.1	11.7	0.2	4.3	9.8	3.6	3.8	0.7	0.33
Vesuvius 1631	53.8	0.6	19.9	4.8	0.1	1.8	6.8	4.7	7.9	0.0	0.28
Erebus melt	58.0	1.0	20.0	5.4	0.2	0.9	2.6	7.1	4.6	0.0	0.08
Vesuvius GP79	55.1	0.5	19.7	4.1	0.1	1.8	5.3	4.4	8.7	0.0	0.27

The calculated NBO/T values of the oxidized melts range from 0.10 to 0.33 (**Table 2**). DR01 and DR10 basanite samples have the highest NBO/T (0.32 and 0.33). On the other hand, DR07 and DR17 phonolite samples have the lowest NBO/T (0.10 and 0.11) related to their higher SiO_2 content. The tephriphonolite has an intermediate NBO/T of 0.20.

3.2. Viscosity data

The viscosity in air for anhydrous and crystal- and bubble-free basanite, tephriphonolite and phonolite melts of the Mayotte submarine volcanic chain are presented as a function of temperature in **Figures 3** and **4** and given in **Table 4**. High-temperatures viscosity was

obtained for all samples while low-temperature viscosity was only obtained for DR07 (**Fig. 3** and **Table 4**). As discussed below, this is because it was not possible to prepare the crystal-free glass samples needed for the low-temperature measurements.

High-temperature viscosity measurements were performed between 1499 K and 1860 K. For each composition, the lower bond of the measurement temperature interval was chosen such that no crystallization was expected. For that, we used the MELTS model (Ghiorso and Sack 1995) that predicts magnetite crystallization below 1573 K for basanite samples. Lower crystallization temperatures were predicted for more differentiated samples. In the super-liquidus temperature range, the relationship between viscosity and temperature is mostly linear (**Fig. 3**), in agreement with previous reports (e.g. Bottinga et al. (1982)). The data are therefore interpolated using the Arrhenius relation:

$$\log_{10}\eta = A_{Arr} + \frac{Ea}{RT}, \quad (2)$$

where η is the melt viscosity (Pa·s), A_{Arr} is a constant, T is temperature (K), R is the gas constant (J mol^{-1} K^{-1}), and E_a is the viscous flow activation energy (kJ mol^{-1}).

For DR07, as we obtained both high- and low-temperatures data (**Fig. 3** and **Table 4**), we use the Vogel-Fulcher-Tamman (VFT; Vogel 1921; Tamman and Hesse 1926; Fulcher 1925) equation to interpolate the viscosity data:

$$\log_{10}\eta = A + \frac{B}{T-C}, \quad (3)$$

with A, B and C the pre-exponential factor, the pseudo-activation energy and the VFT temperature, respectively. The viscosity-temperature variation of the phonolite melts from Vesuvius and Erebus are also shown as comparison (**Fig. 3**).

Table 3. *Viscosity measurements of the basanite-to-phonolite melts along the Mayotte submarine volcanic chain. The uncertainty is equal to or lower than 0.03 log (Pa·s).*

Basanite melt				Tephriphonolite melt		*Phonolite melt*			
DR01		*DR10*		*DR21*		*DR07*		*DR17*	
T (K)	*η* (log_{10} Pa·s)	*T* (K)	*η* (log_{10} Pa·s)	*T* (K)	*η* (log_{10} Pa·s)	*T* (K)	*η* (log_{10} Pa·s)	*T* (K)	*η* (log_{10} Pa·s)
						986	12.30		
						1006	11.61		
						1016	11.30		
						1025	11.00		
						1027	10.87		
						1037	10.67		
						1048	10.44		
						1058	10.19		
								1499	3.89
								1525	3.71
								1551	3.54
								1576	3.37
1595	0.99	1596	1.16	1596	1.97	1597	3.10	1596	3.27
1646	0.79	1648	0.94	1647	1.73	1648	2.80	1646	2.95
1698	0.61	1699	0.74	1696	1.50	1700	2.52	1698	2.67
1749	0.43	1753	0.56			1751	2.25	1750	2.40
1761	0.40			1762	1.23				
				1766	1.20			1766	2.32
1801	0.27	1809	0.38	1809	1.04	1804	2.01	1807	2.12
		1810	0.34						
1855	0.11			1858	0.89	1860	1.75	1855	1.91

At super-liquidus temperatures, the basanite melts have the lowest viscosity (DR01: 0.99 to 0.11 log_{10} Pa·s at 1595 to 1855 K, and DR10: 1.16 to 0.34 log_{10} Pa·s at 1596 to 1810 K) followed by the tephriphonolite (1.97 to 0.89 log_{10} Pa·s at 1596 to 1858 K) and the phonolite melts (DR07: 3.10 to 1.75 log_{10} Pa·s at 1597 to 1860 K, and DR17: 3.89 to 1.91 log_{10} Pa·s at 1499 to 1855 K). **Figure 3** shows that, at temperature between 1500 and 1855 K, the viscosity of the basanite melts differ from those of the phonolite ones by about two orders of magnitude. In particular, at 1750 K, the viscosity is of 0.43, 1.27 (estimated value from **Eq. 2**) and 2.40 log_{10} Pa·s, for the basanite (DR01), tephriphonolite (DR21) and phonolite (DR17) melts, respectively (**Table 3**). At undercooled temperatures, the viscosity of DR07 ranges from 12.3 log_{10} Pa·s at 986 K to 10.2 log_{10} Pa·s at 1058 K (**Fig 3.**).

We compare our measurements to estimates from the Giordano et al. (2008) and Hui and Zhang (2007). Results show that GRD model tends to predict well the viscosity of basanite

melts, while a slight underestimation is observable for the tephriphonolite at high-temperatures (**Fig. 4**). This becomes critical for the phonolite for which the GRD model significantly underestimates the viscosity at both high- and low-temperatures (**Fig. 4**). Conversely, the HZ model tends to slightly overestimate the viscosity of the basanites and tephriphonolites at high-temperatures, and it is in good agreement with the measured viscosity of phonolites at high-temperatures but significantly underestimates the values at low-temperatures (**Fig. 4**). As also shown by Le Losq et al. (2015a) the GRD model underestimates by ~0.5 log units the viscosity of Erebus (**Fig. 4**). In contrast, for the Vesuvius melt, at super-liquidus temperatures there is a difference of less than almost ~0.2 log units between the predicted and the measured viscosity (**Fig. 4A**), while at low-temperatures the GRD model fits well the viscosity data (**Fig. 4B**).

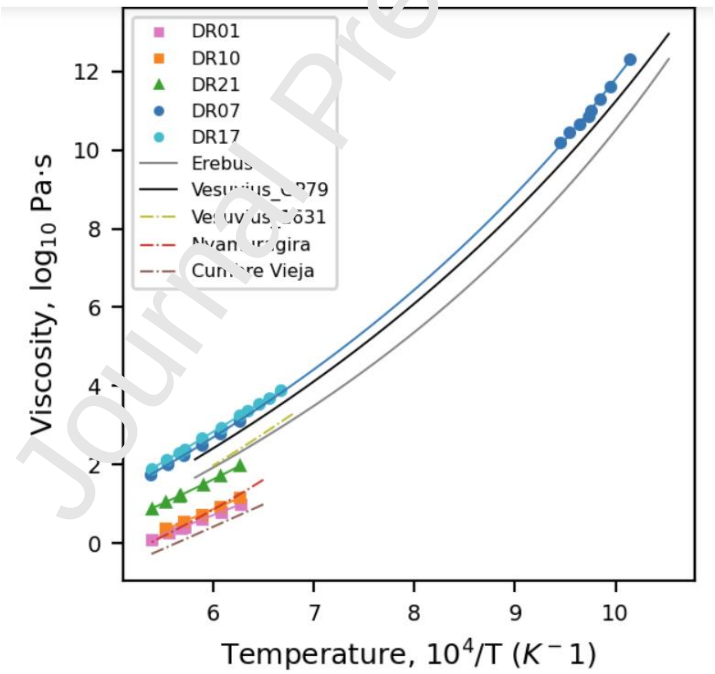

Figure 3. *Viscosity (log_{10} Pa·s) as a function of inverse temperature (K^{-1}) for the Mayotte basanite-to-phonolite magmatic differentiation trend. Squares, diamonds and circles represent measurements made on basanites (DR01 and DR10), tephriphonolite (DR21) and phonolites (DR07 and DR17), respectively. Erebus, Vesuvius GP79 (Giordano et al. 2009; Le Losq et al. 2015a), Vesuvius 1631 (Romano et al. 2003), Cumbre Vieja (Castro and Feisel*

*2022) and Nyamuragira (Morrison et al. 2020) are also represented. Solid and dashed lines are interpolations of the data with the VFT (**Eq. 3, Table 4**) and the Arrhenius equations (**Eq. 2**), respectively. Error bars are smaller than the symbol size.*

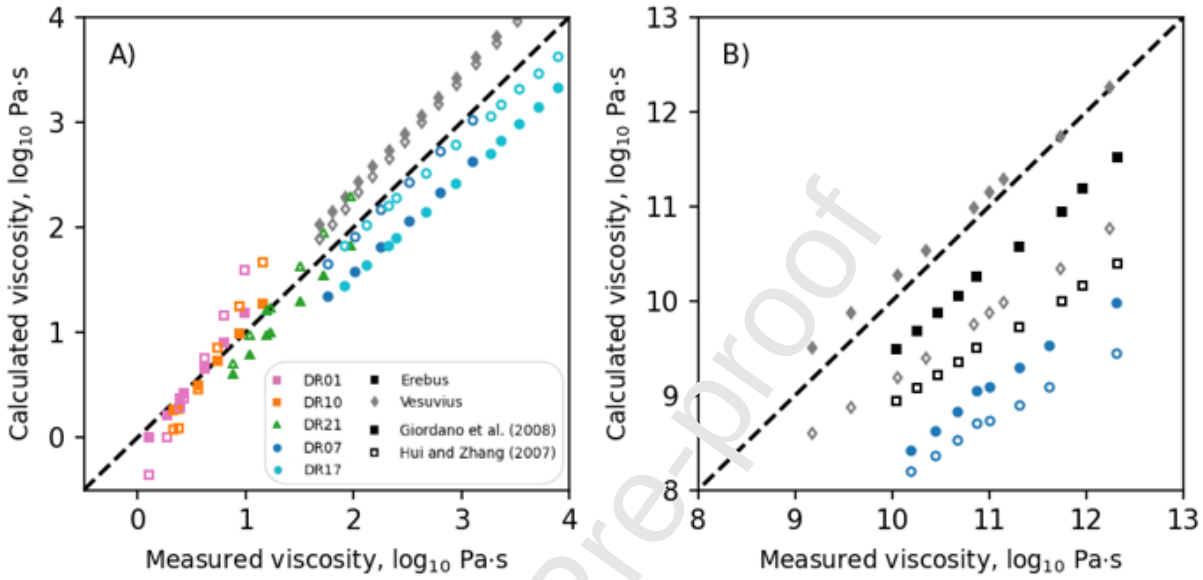

Figure 4. *Comparison between the measured viscosity (log_{10} Pa·s) and the calculated ones with the models of Giordano et al. (2008) (filled symbols) and of Hui and Zhang (2007) (open symbols) in the super-liquidus (A) and undercooled (B) temperature ranges. Error bars are smaller than the symbol size.*

3.3. Raman spectroscopy

To check for crystallization during the low-temperature viscosity experiments, we compare the Raman spectra of DR07 before and after the low-temperature viscosity experiments (**Fig. 5**). Before the experiment, the DR07 glass Raman spectrum exhibits three main broad bands near 80, 490 and 1000 cm^{-1}. The first is the Boson peak assigned to transverse acoustic vibrational modes promoted in silicate glasses by cooperative inter-tetrahedral vibrations (Buchenau et al. 1986; Malinovsky and Sokolov 1986; Hehlen et al. 2002). This is a universal signature of the glassy state (Malinovsky and Sokolov 1986), which tends to quickly

disappear in the presence of crystals (e.g., Takahashi et al. 2009). The second is assigned to inter-tetrahedral T-O-T (T = Si, Al) vibrations in the aluminosilicate network. The third is assigned to intra-tetrahedral T-O stretching vibration (Mysen et al. 1982; McMillan 1984; Le Losq et al. 2014).

After the low-temperature viscometry, the recovered DR07 sample does not show the Boson peak anymore (**Fig. 5**). This indicates that some degree of crystallization must have occurred during the viscosity measurements near the glass transition.

We also acquired Raman spectra on all the other samples quenched during the initial glass preparation (see supplementary **Fig. A1**). Although microscopic inspection of the samples appeared crystal-free, and although the Raman spectra above 200 cm^{-1} may not present sharp peaks typical of crystals, no Boson peak was visible. This indicates that initial glass samples other than DR07 contained crystals at a sub-nanometric to nanometric scale (see Discussion). Interestingly, we did not succeed to obtain a pure glass for the DR17 phonolite despite a very similar chemical composition with DR07. This may be explained by the slightly higher Na_2O and Al_2O_3 contents that could be responsible for a different behavior. This testifies that crystal-free glass basanite, tephriphonolite and phonolite samples of the required size for low temperature viscosmetry are extremely difficult to obtain.

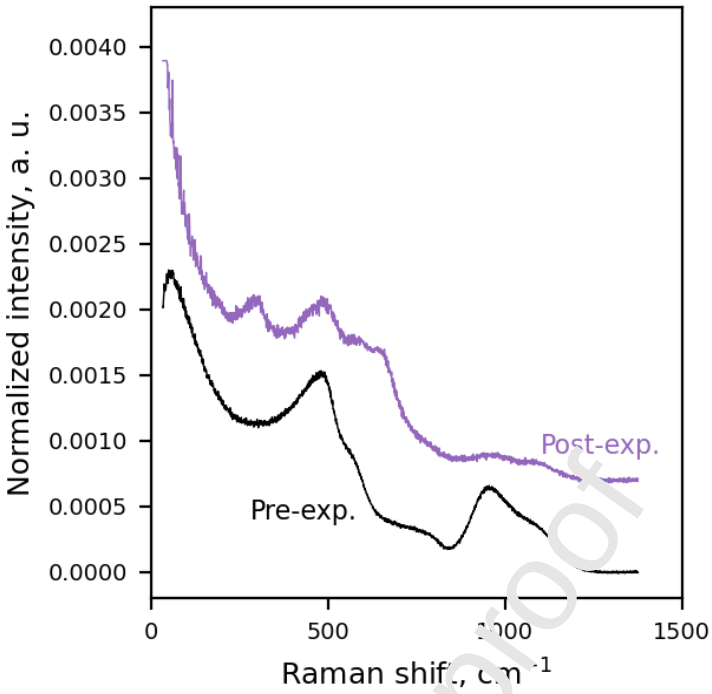

Figure 5. *Uncorrected Raman spectra of DR07 phonolite products pre (black curve)- and post (purple curve)-experiments at low-temperature.*

4. Discussion

4.1. *Nanolite crystallization during low-temperature measurements*

DR07 is the only sample for which we obtained a glassy piece large enough to perform near-T_g viscometry. However, during the experiment, the sample seems to have undergone some degree of crystallization as evidenced by the disappearance of the Boson peak (**Fig. 5**). To confirm that crystallization occurred, we acquired a scanning transmission electron microscope (STEM) image with the Helios 5 (ThermoFisher Scientific) scanning electron microscope coupled with a focused ion beam (Xe plasma FIB-SEM) at LMV. Images show the presence of homogeneously distributed brighter particles at the nanoscale (**Fig. 6**). Similar particles with a size ranging from 5 to 30 nm have been observed and characterized as nanolites (Di Genova et al. 2017, 2018, 2020).

The effect of crystallization on viscosity may reach several orders of magnitudes (e.g., Lejeune et Richet, 1995; Costa et al. 2009; Mader et al. 2013), particularly in presence of microlites (Del Gaudio et al. 2013) or nanolites (Di Genova et al. 2020; Le Losq et al. 2021a). In the present case, we observe neither a deviation of the viscosity measurements as a function of time nor the apparition of a non-Newtonian behavior. Therefore, it seems that the presence of nanolites only has limited effects on our measurements. However, this finding suggests that nanolite crystallization happens very quickly in melts of iron-bearing alkaline compositions and even in silica-rich melts such as phonolites. To check for this, we placed a DR07 glassy sample in an annealing furnace and setup the temperature at the glass transition, with a particular care in avoiding overshooting while checking the sample temperature with a Pt-PtRh10% type S thermocouple placed in contact with the sample. The Raman spectra of the retrieved sample also showed the presence of crystals in the glass after annealing, and is actually identical to that of the post-experiment viscometry sample shown in **Figure 5**.

These findings suggest that previously published viscosity measurements for iron-bearing alkali compositions in the undercooled temperature domain (e.g., Giordano et al. 2000, 2005; Giordano and Dingwell 2003; Le Losq et al. 2015a) may probably have been also affected by nanolite formation. As the first nanolites to appear are Fe-Ti oxides, we hypothesize that this mostly affects iron-bearing compositions, explaining the choice of some authors to work with iron-free melts (e.g., Whittington et al. 2000, 2001). Because diffusion increases with decreasing Si content (Zhang and Ni 2010), we further stress that this effect is expected to be even stronger for tephriphonolite and basanite composition, preventing pure glass samples from being obtained. Great care should therefore be taken during low-temperature viscometry even for phonolite melt, and Raman spectra down to the Boson peak wavelength range or X-ray Diffraction spectra should be systematically acquired after experiments to check for sample crystallization.

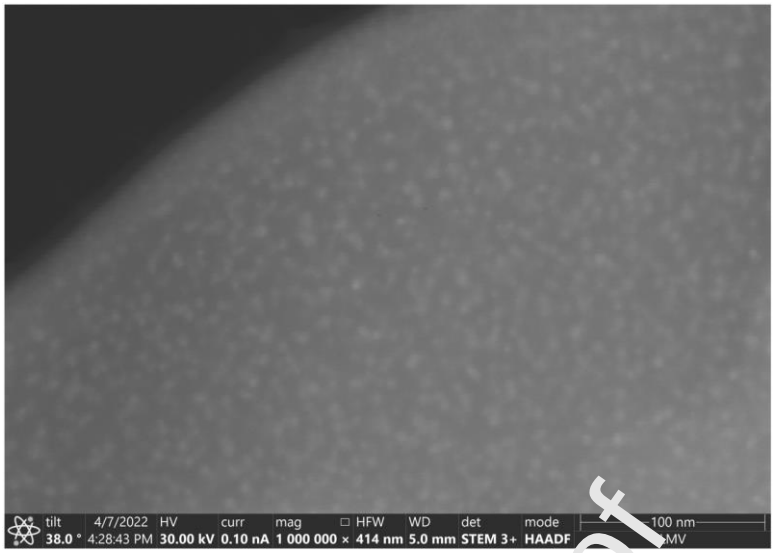

Figure 6. *Scanning transmission electron microscope image of the DR07 sample post low-temperatures viscosity measurements.*

4.2. ***Melt viscosity and comparison with models***

A discrepancy between experimental measurements and parametric viscosity models, as observed here (**Fig. 4**), has also been previously reported for alkaline composition by Le Losq et al. (2015a). There are two likely causes for the significant difference between the GRD model and the measured viscosity at low-temperature. First, unlike at high-temperatures, in undercooled melts, important and nonlinear variations in melt configurational entropy result from changes in melt composition (Richet 1984; Neuville and Richet 1991; Le Losq et al. 2021a). This drives important changes in melt viscosity, challenging to reproduce with parametric models. Therefore, this could explain the discrepancy between the GRD model and our low-temperature viscosity measurements. Secondly, the GRD model has been calibrated with a restricted alkaline basanite-to-phonolite compositional data subset (Giordano et al. 2008). This could reduce the accuracy of the viscosity prediction of this model for such compositions. This also explains why the Vesuvius melt is better reproduced

as this composition was part of the database used to parametrize the GRD model (Giordano et al. 2008).

Additional comparison has been performed between our viscosity measurements and the predictions from the Hui and Zhang (2007) model. The HZ model is in relatively good agreement with our viscosity measurements at high-temperatures (**Fig. 4A**) whereas it significantly underestimates between 2 and 3 $\log_{10}$ units the viscosity of phonolite melt at low-temperatures (**Fig. 4B**). Similar differences are observed between the HZ model and the measurements made on other phonolite melts from Erebus (Le Losq et al. 2015a) and Vesuvius GP79 (Giordano et al. 2009; Le Losq et al. 2015a). According to Hui and Zhang (2007), the model could be improved in part by adding new viscosity measurements at low-temperatures and by considering the effect of ferric and ferrous iron. Also, as for the GRD model, the HZ model is a general model leading to an increase in uncertainty for specific compositions.

In order to refine such pre-existing models and thus improve their accuracy in the viscosity prediction, it is important to keep measuring natural samples. The present viscometry data could then be used to improve such models.

4.3. ***Polymerization and viscosity***

The relationships between super-liquidus viscosity and melt polymerization, in terms of T-O-T bridging as quantified by the chemically-derived, oxidized NBO/T (**Eq. 1**), are illustrated in **Figure 7**. At given temperature, basanite melts show the lowest viscosity (< 1.2 $\log_{10}$ Pa·s) and the highest NBO/T (0.32 to 0.33) whereas phonolite melts have the highest viscosity (> 2 $\log_{10}$ Pa·s) and lowest NBO/T (0.10 and 0.11) (**Fig. 7**). Accordingly, the tephriphonolite sample, having an intermediate chemical composition (**Fig. 2** and **Table 2**), falls in between the basanite and phonolite compositions (**Fig. 7**). The fact that the highest viscosity data are obtained for the samples with the lowest NBO/T, and inversely, is an expected pattern

(Mysen et al. 1982, 1985; Scarfe et al. 1987; Mysen and Richet 2019). A higher degree of polymerization (lower NBO/T) will lead to lesser solutions for performing the cooperative rearrangements of the molecular sub-units necessary for melt viscous flow. According to the Adam-Gibbs theory of viscous flow, this results in a lower melt configurational entropy and, hence, in a higher melt viscosity (Adam and Gibbs 1965; Richet 1984). Such variations in melt polymerization with composition, albeit expected, may have an important impact on the eruptive style (see Implications section).

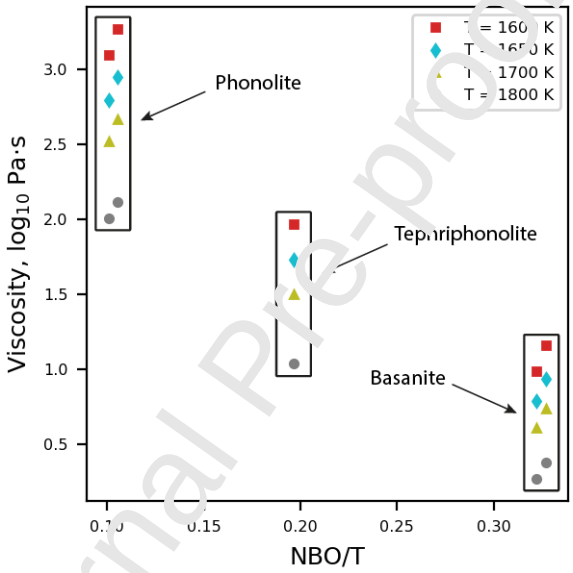

Figure 7. *Variations of the viscosity (log_{10} Pa·s) at a given temperature relative to composition as represented by the ratio of non-bridging oxygen to tetrahedrally-coordinated cations (NBO/T). See also* ***Tables 2*** *and* ***3*** *for chemical compositions and viscosity results, respectively.*

4.4. Influence of iron redox state and volatile concentration on melt viscosity

All the presently reported experiments were performed in air. In addition, we measured the viscosity of volatile-free melts, as they degassed upon preparation. Therefore, to provide accurate viscosity estimates of the basanite, tephriphonolite and phonolite lavas in a natural

context, we should take into account the influence of both water and iron oxidation state on the viscosity of the silicate melts. Fe^{3+} reduction to Fe^{2+} can lead to decreasing melt viscosity of 0.2 - 0.5 log units at super-liquidus conditions; this effect can reach up to 1.5 log units at undercooled temperatures (Dingwell and Virgo 1987; Dingwell 1991; Liebske et al. 2003; Chevrel et al. 2013). Water also strongly participates in lowering the viscosity of alkaline magmas (e.g., Whittington et al. 2000, 2001).

To quantify the effect of water, we here follow the methodology of Le Losq et al. (2015a) who calculated the relative effect of water on the B and C terms of the VFT equation (**Eq. 3**) for phonolite melts, based on previously published data from Whittington et al. (2001). In that way, we use the following equation:

$$log_{10}\,\eta = A + (B^{anh} + K_1 * C_{H2O} + K_2 * C_{H2O}^2) / (T - (C^{anh} + K_3 * C_{H2O} + K_4 * C_{H2O}^2)), \quad (4)$$

where K_1, K_2, K_3 and K_4 are the parameters of the polynomial functions that describe the effect of the water concentration in wt%, C_{H2O}, on the value of the parameters B and C. B^{anh} and C^{anh} are the VFT B and C parameters of the anhydrous melt. Regarding the basanite composition, no viscosity measurements at undercooled temperatures were obtained for this study. Hence, we calculated the VFT parameters of the anhydrous melt by combining our high-temperature data with the low-temperature data estimated from the GRD model (**Table 4**). To calculate the K_1, K_2, K_3 and K_4 parameters, we then used the VFT parameters published by Whittington et al. (2000) for a hydrous iron-free basanite. **Table 5** reports the K_1, K_2, K_3 and K_4 parameters from Le Losq et al. (2015a).

Table 4. *Parameters obtained for Arrhenius relation at high-temperature (**Eq. 2**) and VFT parameter over the entire temperature range (**Eq. 3**). The VFT parameters calculated for the*

basanite DR10 result from a combination of the high temperatures data from this study and low-temperatures estimated from the GRD model (see Discussion).

Sample	Temperature range (K)	Viscosity range (log_{10} Pa·s)	A_{Arr}	Ea_{Arr} (kJ mol^{-1})	$RMSE_{Arr}$	A_{VFT}	B_{VFT}	C_{VFT}	$RMSE_{VFT}$
DR01	1600 - 1855	0.99 - 0.11	-5.34	44.37	0.003	-	-	-	-
DR10	1600 - 1810	1.16 - 0.34	-5.6	46.57	0.015	-4.6	6053.1	573.64	0.05
DR21	1600 - 1860	1.97 - 0.89	-5.8	48.23	0.011	-	-	-	-
DR17	1500 - 1855	3.89 - 1.91	-6.46	53.72	0.008	-	-	-	-
DR07	990 - 1860	12.30 - 1.75	-	-	-	-3.9	7572	517	0.04

Table 5. *K parameters for estimating the effect of water on the parameters B and C of the VFT equation (**Eq. 4**) for the phonolite (from Le Losq et al. 2015a) and the basanite (this study).*

Parameters	Values for phonolite DR07	Values for basanite DR10
K_1	-455.52	-103.15
K_2	32.626	133.87
K_3	-110.61	-140.77
K_4	13.241	32.043

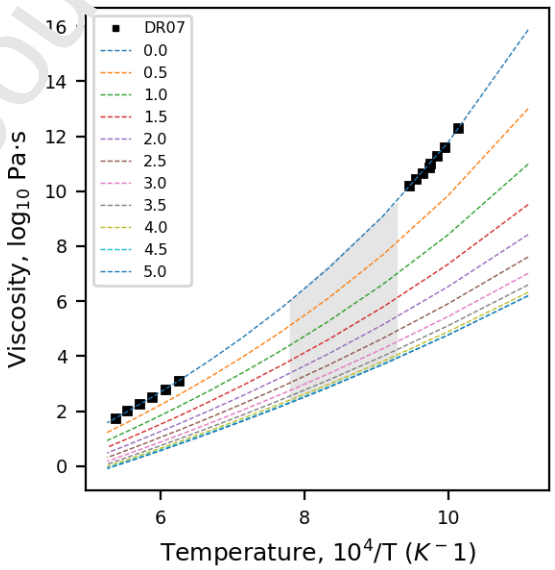

Figure 8. *Viscosity (log_{10} Pa·s) as a function of inverse temperature (K^{-1}) for the DR07 phonolite. Measured viscosity values (squares) are shown together with values predicted (curves) by* ***Eq. 4*** *for different water concentrations (wt %). Numbers in the label refer to water content in wt% and the expected magmatic conditions are indicated by the grey box. The 4.5 and 5.0 wt% water curves are superposed. Error bars are smaller than the symbol size.*

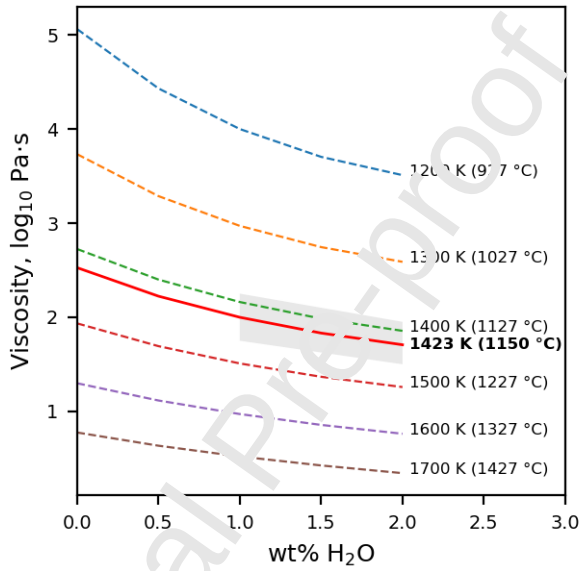

Figure 9. *Isothermal viscosity as a function of water concentration (wt%) for the DR10 basanite. The predicted magmatic conditions proposed by Berthod et al. (2021b) are indicated by the red line (1150 °C) and its uncertainty by the grey box (± 50 °C).*

We present the effect of water on the phonolite (DR07) in **Figure 8** and on the basanite (DR10) in **Figure 9**. As expected, the water strongly lowers the viscosity for both melts. The addition of 1 wt% of water reduces the viscosity from 2.50 to 1.68 log_{10} Pa·s at 1700 K for the DR07 phonolite. The decreasing effect of water on viscosity is higher at lower temperatures, where the difference between anhydrous and hydrous melts may reach up to 4 orders of magnitude at 900 K (**Fig. 8**). In contrast, the addition of 1 wt% of water decreases the viscosity of the basanite by almost 0.3 log_{10} units at 1700 K (**Fig. 9**). This analysis shows

that (i) further addition of water results in a progressively less important decrease in viscosity and (ii) the effect of water is more effective at reducing the viscosity of polymerized melts (phonolites) than for depolymerized melts (basanites). As it has been previously demonstrated, the chemical composition of the melt affects water solution mechanisms, resulting in different effects on melt structure (e.g., Whittington et al. 2000, 2001; Xue and Kanzaki 2004, 2006; Cody et al. 2005; Mysen and Cody 2005; Mysen and Richet 2005; Giordano et al. 2009; Le Losq et al. 2015b). For polymerized melts, the proposed water solution mechanism is the reaction of water molecules with the silicate network, breaking T-O-T bonds (with T = Si, Al) (e.g., see Mysen and Richet 2019; Le Losq et al. 2015b). In contrast, in depolymerized melts, water molecules may react with network modifiers (e.g., Ca, Mg), leading to reduced or no changes in melt polymerization (Xue and Kanzaki 2004; Moretti et al. 2014; Le Losq et al. 2015b). The present basanite and phonolite show relatively low NBO/T values. Therefore, water solution should imply mostly reaction of water molecules with T-O-T bridges, and result in melt depolymerization. A stronger depolarization effect may be expected for phonolites because of their higher activity of silica, which should lead to higher reaction rates between Si-O-Si bridges and water. This may explain the predicted behavior of viscosity variations with water content in the different melts (**Figs. 8 and 9**).

To conclude on this part, considering the above discussion and in particular the fact that we measured the viscosity of oxidized melts, the reported viscosity values represent upper limits for aluminosilicate melts due to the effect of water combined with the iron oxidation state.

4.5. ***Comparison of crystal-free melts from different areas***

Only a few studies present viscosity of natural basanites (e.g.; Castro and Feisel 2022; Morrison et al. 2020). The crystal-free melt (remelted lava) from the 2021 eruption of Cumbre Vieja (La Palma) has a viscosity of 0.83 $\log_{10}$ Pa·s at 1573 K (Castro and Feisel

2022). At this temperature, the estimated viscosity by using the Arrhenian fit is 1.08 and 1.26 $\log_{10}$ Pa·s for the DR01 and DR10 melts highlighting a higher viscosity (**Figs. 3 and 10**). At 1595 K, we obtained 0.99 and 1.16 $\log_{10}$ Pa·s for DR01 and DR10 samples, respectively (**Table 3**). By contrast, at 1590 K, the viscosity of the basanite from the 1948 Nyamuragira (Democratic Republic of Congo) eruption is 1.27 $\log_{10}$ Pa·s (Morrison et al. 2020) that is clearly more viscous than the one from Fani Maoré (**Fig. 3**). This difference may be explained by variations in chemical compositions, with the basanite from Cumbre Vieja containing a lower SiO_2 (44 – 46 wt%) and a higher CaO (9.4 – 11.1 wt%) contents than Fani Maoré and Nyamuragira (**Fig. 2**). According to previous studies (e.g.; Mysen et al. 1980; Mysen 1995; Richet et al. 1984; Stebbins et al. 1992; Stebbins and Xu 1997), the alkaline-earth elements (Mg and Ca) may act as network modifiers and favor the creation of non-bridging oxygen (NBO) atoms and, hence, a decrease in viscosity. In the other hand, the Nyamuragira basanite is enriched by 1.2 wt% in K_2O (Morrison et al. 2020) compared to the basanites from Mayotte and La Palma (**Table 2**). In Al-rich melts, addition of K_2O can lead to decreasing the melt configurational entropy and so, to increasing its viscosity at constant temperature as observed in **Figure 10** (Le Losq et al. 2013, 2017, 2021b; Robert et al. 2019). Therefore, the variation in concentration of these few elements between these basanites could explain the observed viscosity distinctions.

The viscosity data of the tephriphonolite from Mayotte is compared to the viscosity measurements of the AD 1631 Vesuvius (Romano et al. 2003). The viscosity of the AD 1631 Vesuvius tephriphonolite ranges from 1.96 to 2.56 $\log_{10}$ Pa·s between 1670 and 1572 K (Romano et al. 2003) whereas, we expect a viscosity from 1.61 to 2.10 $\log_{10}$ Pa·s at these temperature range for the tephriphonolite from Mayotte (**Figure 3 and Table 3**). The K_2O content (7.91 – 8.28 wt%) twice as high in the AD 1631 Vesuvius sample (Romano et al. 2003) may explain its higher viscosity (**Fig. 10**).

We can also compare the viscosity of the phonolites from Mayotte (DR07 and DR17) to data from previous studies on similar Al- and alkali-rich compositions like the phonolite from Erebus (Le Losq et al. 2015a) and from Vesuvius GP79 (Giordano et al. 2009; Le Losq et al. 2015a) (**Fig. 3**). The viscosity of the Vesuvius GP79 sample is lower by an order of magnitude compared to the phonolite from the East-Mayotte submarine volcanic chain. This may be explained by a lower SiO_2 content (54 wt% against 59 wt%). Despite a similar composition in SiO_2 and alkali elements (**Fig. 2** and **Table 2**), the viscosity of DR07 differs from the Erebus one by about 0.5 orders of magnitude. The phonolites of Mayotte (DR07 and DR17) are richer by 1 to 2 wt% of iron compared to the Erebus sample (**Table 2**). In contrast to Chevrel et al. (2013), a decrease in melt viscosity with increasing iron concentration is not observed. As for the basanites and tephriphonolites, the observed viscosity difference more probably finds its origin in variations in the concentrations of a few elements such as K, Mg and Ca between the phonolites of Mayotte and Erebus. Indeed, the DR07 and DR17 samples are slightly more enriched in K_2O (**Table 2**) whereas the Erebus sample contains a bit more alkaline-earth elements (Mg and Ca). Hence, it seems consistent that the DR07 phonolite from Mayotte has a higher viscosity than the Erebus sample. As explained previously, no viscosity measurements at undercooled temperatures could be obtained for the DR17 phonolite. However, according to the viscosity at super-liquidus temperatures and the enrichment in alkali (**Figs. 2 and 3**) we may assume that the viscosity at undercooled temperatures will be higher than the DR07, Erebus and Vesuvius melts.

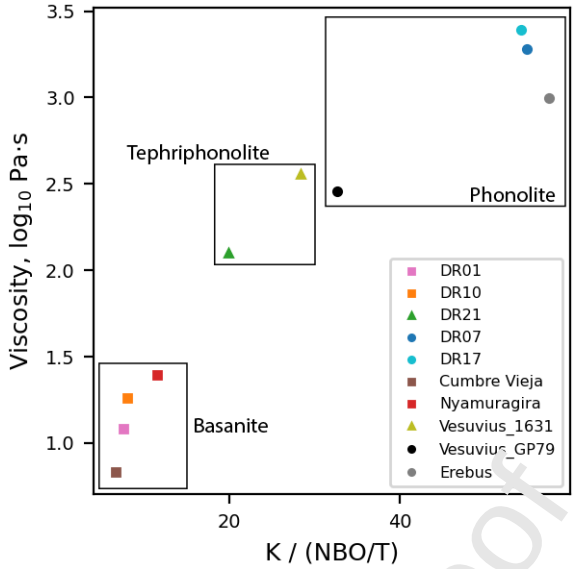

Figure 10. *Viscosity (log_{10} Pa·s) as a function of K / (NBO/T) ratio at 1573 K for the Mayotte basanite-to-phonolite magmatic differentiation trend. Erebus and Vesuvius GP79 (data from Giordano et al. 2009; Le Losq et al. 2015a), Cumbre Vieja (Castro and Feisel 2022), Nyamuragira (Morrison et al. 2020) and Vesuvius 1631 (Romano et al. 2003) are also represented.*

5. Implication on eruption dynamics

Upon magma ascent in a conduit, the style of a volcanic eruption depends on whether the magma fragmentation threshold is crossed (explosive) or not (effusive). This threshold will depend on the magma viscosity but also on the ascending rate and bubble overpressure (e.g., Dingwell et al. 1996; Papale 1999; Ma et al. 1999; Pistolesi et al. 2011; Gonnermann et al. 2011; Gonnermann 2015). Generally, in magmas with high viscosity (silica-rich composition), the enhanced resistance to bubble expansion favors bubble overpressure and reduces the ability of volatiles to stream out of the melt. This in turn promotes more efficient magma fragmentation and a greater explosivity of eruptions. Of course, many exceptions break such general rules, such as basaltic Plinian eruptions (e.g., Moitra et al. 2018) and Si-

rich lava flows (e.g., Fink 1983; Farquharson et al. 2015; Prival 2022, Ramírez-Uribe et al. 2022). Additionally, eruption style can switch between effusive and explosive activities during an eruption due to variations in magma composition, degassing, and crystallization that all drive magma viscosity (e.g., Vesuvius Giordano et al. 2009; Myers et al. 2021, Andújar and Scaillet 2012; Popa et al. 2021). Attempts have been done to define the viscosity threshold to discriminate explosive to effusive eruptions, but no consensus has yet been achieved (Papale 1999; Di Genova et al. 2017; Wadsworth et al. 2018).

Our results show that basanite melts have the lowest viscosity of the series followed by the tephriphonolite and the phonolite melts and that the presence of water reduces the viscosity. The very low crystal content (up to 6%) of the Fani Maoré lavas (Berthod et al. 2021a) should not be sufficient to significantly affect the viscosity. However, the lavas include an average of 35% of vesicles (Berthod et al. 2021b), which could likely decrease the viscosity of the melt and hence the presented viscosity here are probably upper limits. Assuming that the eruptive temperature (T_e) of the Fani Maoré basanite lavas is around 1150 °C (Berthod et al. 2021b), and that water content could range from 1.0 to 2.3 wt% (Berthod et al. 2021b), we thus expect crystal- and bubble free lava viscosity upon eruption to range from 1.8 to 2.1 $\log_{10}$ Pa·s (**Fig. 9**). Such a viscosity range is close to, for example, the viscosity of subaerial pahoehoe basaltic lavas from Hawaii (Chevrel et al. 2018) or submarine basaltic lava flows (McClinton et al. 2014). This low viscosity range is therefore consistent with the effusive eruption style and morphologies (pillow lavas and pahoehoe lavas) of the lava flow field as observed at Fani Maoré (Feuillet et al. 2021; Berthod et al. 2021b). However, several questions remain. Can the basanite magma low viscosity favor undirect lava flow path that could explain the location of the Fani Maoré eruptive site that is shifted by 30 km from the supposed magmatic chamber (Berthod et al. 2021b, Lemoine et al. 2020; Feuillet et al.

2021)? Could the low viscosity favor the high flux rates (150 – 200 m^3 s^{-1} averaged over the first year, Berthod et al. 2021b) and the long duration eruption if the volume was there? ?

Around the Horseshoe volcanic site of the Mayotte volcanic chain, a large diversity of edifice morphologies and deposits textures corresponding to both phonolite effusive and explosive eruptions have been observed (REVOSIMA 2022; Puzenat et al. 2023; Gurioli et al. 2023; Komorowski et al. 2023). Such diversity can be explained by the fact that, depending on magma ascent rates, eruptive temperatures and initial water contents, phonolite magmas can be involved in a broad range of magmatic effusive and explosive activity (e.g., see Andújar and Scaillet 2012). Indeed, the Mayotte phonolite magmas evolved from basanite magma by ~80% of fractional crystallization (Berthod et al. 2021a). They are expected to present a high viscosity at expected eruption temperatures (typically in the 800-1000 °C range, e.g. see Andújar and Scaillet 2012). However, phonolite magmas are also expected to contain a large amount of dissolved water. If assuming a phonolite magma stored in a deep reservoir at T_e = 800 - 1000 °C and containing ~5 wt% water (Andújar and Scaillet 2012), this magma could have a viscosity as low as 2.0 - 3.8 log_{10} Pa·s (**Fig. 8**), not that far from that previously estimated for the basanite melt. However, upon migration toward the surface, vigourous water exsolution is expected to occur. According to the composition of the submarine phonolites from Mayotte (encountered at 1,300 to 1,600 m b.s.l.), the residual water content in erupted phonolite glass ranges between 0.8 and 1.2 wt% (Thivet et al., under review). Considering such values, the viscosity of the phonolite melts may increase of up to 2 to 3 orders of magnitudes upon ascent (**Fig. 8**). In parallel, the significant water exsolution will lead to the formation of a magmatic foam of low density in the conduit, reinforcing the buoyant force that pushes the magma out toward surface. This effect is particularly promoted in silica-rich melts like phonolites, because their high viscosity favors entrapment of bubbles (Thomas et al. 1994; Gardner et al. 1996). Therefore, exsolution of water from such

magmatic liquids often results in foaming, largely enhancing the probability of brittle fragmentation of the foam (Jones et al. 2019; Scheu and Dingwell 2022) in the conduit (e.g., Dingwell 1996; Papale 1999; Gonnerman, 2015). Therefore, the amount of water initially stored in the chambers will determine the eruptive styles (Andújar and Scaillet 2012; Popa et al. 2021). The occurrence of both effusive and explosive phonolite eruptions at Mayotte, testified by the observed deposits and products, indicate that a broad range of storage conditions and degassing history exist along this volcanic chain, leading to open questions regarding the future events that could imply phonolite melts.

6. Conclusion

This study provides precise quantification of the temperature-viscosity relationship for basanite to phonolite melts through a large temperature range and discusses the effect of dissolved water on melt viscosity. We show that at eruption temperatures basanite lavas are more propitious to erupt in an effusive manner while phonolite may erupt effusively or explosively. However, we do not account for the effect of bubbles and crystals on magma viscosity. Future studies should account for their effect to provide a holistic view of magma rheology which directly impacts the dynamics and eruption style as well as lava flow emplacement. For this, detailed sample texture analyses should be undertaken on collected samples to quantify the bubble and crystal content, shape, size and distribution that are necessary to constrain magma suspension rheology (see Harris and Allen 2008; Mader et al. 2013; Kolzenburg et al. 2022). Measuring the viscosity of magmatic liquids along the Mayotte alkali magmatic differentiation trend combined with known volatile content, and crystal and bubbles characteristics, is essential to quantify the evolution of magma viscosity during ascent rate, outgassing and crystallization, which directly influence the prevailing conditions determining the eruptive style (whether it is effusive or explosive).

Acknowledgments

MAYOBS 1 campaign was funded by the CNRS-INSU TELLUS MAYOTTE program (SISMAYOTTE project). MAYOBS 1, 2, 4 and 15 campaigns were conducted by several French research institutions and laboratories (IPGP/CNRS/BRGM/IFREMER/IPGS). All marine operations are performed as part of the MAYOBS set of campaigns (https://doi.org/10.18142/291) and we thank the captains and crews of the R/V Marion Dufresne (TAAF/IFREMER/LDA), R/V *Pourquoi Pas?* (GENAVIR/IFREMER, SHOM). We thank the mission chiefs of the MAYOBS campaigns (E. Rinnert, N. Feuillet, Y. Fouquet, S. Jorry, I. Thinon, E. Lebas, F. Paquet) and of the GeoFlamme oceanographic campaign (CNFH; PI C. Cathalot, E. Rinnert, N. Feuillet) for conducting marine operations that benefited this study and provided dredge samples. We also thank additional scientists on board the MAYOBS cruises that conducted the dredge operations and processed the samples (P. Besson, M. Bickert, P. Burckel, B. Caron, C. Deplus, S. Hidalgo, A. Le Friant, S. Nowak). We thank A. Peltier (OVPF-IPGP) and C. Mucig (BRGM Mayotte) respectively the Operational Leader and Co-leader of the REVOSIMA. We thank the scientists of REVOSIMA consortium for access to data and for discussions during the Scientific and Technical Committee meetings. Analyses were funded by the Service National d'Observation en Volcanologie (SNOV, INSU) and the Réseau de Surveillance Volcanologique et Sismologique de Mayotte (REVOSIMA), a partnership between the Institut de Physique du Globe de Paris (IPGP), the Bureau de Recherches Géologiques et Minières (BRGM), and the Observatoire Volcanologique du Piton de la Fournaise (OVPF-IPGP), the Centre National de la Recherche Scientifique (CNRS), and the Institut Français de Recherche pour l'Exploitation de la Mer (IFREMER). Since June 2019, all activities on Mayotte are funded by le ministère de l'Enseignement Supérieur, de la Recherche et de l'Innovation (MESRI), le Ministère de la

Transition Ecologique (MTE), le Ministère des Outremers (MOM), le Ministère de l'Intérieur (MI), and le Ministère des Armées with the support of the DIRMOM (Direction Interministérielle aux Risques Majeurs en Outremer) and the MAPPPROM (Mission d'appui aux politiques publiques pour la prévention des risques majeurs en Outremer). We thank the IPGP for general funding to the Observatoires Volcanologiques et Sismologiques (OVS). The data contributes to the Service National d'Observation en Volcanologie (SNOV). The authors would like to thank IFREMER for their welcome during the sampling and E. Humler for his support and national funding coordination (CNRS, REVOSIMA). The authors also thank Thivet S. for the discussion about the water content within the submarine volcanic samples from Mayotte. The authors want also to thank the reviewers for their constructive comments that improved the first version of this paper. Raman and viscosity measurements were supported *in kind* by funds from the IPGP Geomaterial group. This work contributes to IdEx Université de Paris ANR-18-IDEX-0001 (Chaire d'Excellence to C. Le Losq). This project has received funding from the Institut de Recherche pour le Développement (IRD) and the French Government Laboratory of Excellence initiative no. ANR-10-LABX-0006. This is Laboratory of Excellence ClerVolc contribution n° 577.

References Cited

Adam, G., Gibbs, J.H., 1965. On the Temperature Dependence of Cooperative Relaxation Properties in Glass-Forming Liquids. J. Chem. Phys. 43, 139–146. https://doi.org/10.1063/1.1696442

Andújar, J., Scaillet, B., 2012. Relationships between pre-eruptive conditions and eruptive styles of phonolite–trachyte magmas. Lithos 152, 122–131. https://doi.org/10.1016/j.lithos.2012.05.009

Bachèlery, P., Hémond, C., 2016. Geochemical and Petrological Aspects of Karthala Volcano, in: Bachelery, P., Lenat, J.-F., Di Muro, A., Michon, L. (Eds.), Active Volcanoes of the Southwest Indian Ocean, Active Volcanoes of the World. Springer Berlin Heidelberg, Berlin, Heidelberg, pp. 367–384. https://doi.org/10.1007/978-3-642-31395-0_23

Bachelery, P., Lenat, J.-F., Di Muro, A., Michon, L. (Eds.), 2016. Active Volcanoes of the Southwest Indian Ocean: Piton de la Fournaise and Karthala, Active Volcanoes of the World. Springer Berlin Heidelberg, Berlin, Heidelberg. https://doi.org/10.1007/978-3-642-31395-0

Behrens, H., Roux, J., Neuville, D.R., Siemann, M., 2006. Quantification of dissolved H2O in silicate glasses using confocal microRaman spectroscopy. Chem. Geol. 229, 96–112. https://doi.org/10.1016/j.chemgeo.2006.01.014

Berthod, C., Komorowski, J.-C., Gurioli, L., Médard, E., Bachèlery, P., Besson, P., Verdurme, P., Chevrel, O., Di Muro, A., Peltier, A., Devidal, J.-L., Nowak, S., Thinon, I., Burckel, P., Hidalgo, S., Deplus, C., Loubrieu, B., Pierre, D., Bermell, S., Pitel-Roudaut, M., Réaud, Y., Fouchard, S., Bickert, M., Le Friant, A., Paquet, F., Feuillet, N., Jorry, S.L., Fouquet, Y., Rinnert, E., Cathalot, C., Lebas, E., 2022. Temporal magmatic evolution of the Fani Maoré submarine eruption 50 km east of Mayotte revealed by in situ sampling and petrological monitoring. Comptes Rendus Géoscience 354, 1–29. https://doi.org/10.5802/crgeos.155

Berthod, C., Médard, E., Bachèlery, P., Gurioli, L., Di Muro, A., Peltier, A., Komorowski, J.-C., Benbakkar, M., Devidal, J.-L., Langlade, J., Besson, P., Boudon, G., Rose-Koga, E., Deplus, C., Le Friant, A., Bickert, M., Nowak, S., Thinon, I., Burckel, P., Hidalgo, S., Kaliwoda, M., Jorry, S.J., Fouquet, Y., Feuillet, N., 2021a. The 2018-ongoing Mayotte submarine eruption: Magma migration imaged by petrological monitoring. Earth Planet. Sci. Lett. 571, 117085. https://doi.org/10.1016/j.epsl.2021.117085

Berthod, C., Médard, E., Di Muro, A., Hassen Ali, T., Gurioli, L., Chauvel, C., Komorowski, J.-C., Bachèlery, P., Peltier, A., Benbakkar, M., Devidal, J.-L., Besson, P., Le Friant, A., Deplus, C., Nowak, S., Thinon, I., Burckel, P., Hidalgo, S., Feuillet, N., Jorry, S., Fouquet, Y., 2021b. Mantle xenolith-bearing phonolites and basanites feed the active volcanic ridge of Mayotte (Comoros archipelago, SW Indian Ocean). Contrib. Mineral. Petrol. 176, 75. https://doi.org/10.1007/s00410-021-01833-1

Bottinga, Y., Weill, D., Richet, P., 1982. Density calculations for silicate liquids. I. Revised method for aluminosilicate compositions. Geochim. Cosmochim. Acta 46, 909–919. https://doi.org/10.1016/0016-7037(82)90047-3

Bottinga, Y., Weill, D.F., 1972. The viscosity of magmatic silicate liquids; a model calculation. Am. J. Sci. 272, 438–475. https://doi.org/10.2475/ajs.272.5.438

Buchenau, U., Prager, M., Nücker, N., Dianoux, A.J., Ahmad, N., Phillips, W.A., 1986. Low-frequency modes in vitreous silica. Phys. Rev. B 34, 5665–5673. https://doi.org/10.1103/PhysRevB.34.5665

Castro, J.M., Feisel, Y., 2022. Eruption of ultralow-viscosity basanite magma at Cumbre Vieja, La Palma, Canary Islands. Nat. Commun. 13, 3174. https://doi.org/10.1038/s41467-022-30905-4

Cesca, S., Letort, J., Razafindrakoto, H.N.T., Heimann, S., Rivalta, E., Isken, M.P., Nikkhoo, M., Passarelli, L., Petersen, G.M., Cotton, F., Dahm, T., 2020. Drainage of a deep magma reservoir near Mayotte inferred from seismicity and deformation. Nat. Geosci. 13, 87–93. https://doi.org/10.1038/s41561-019-0505-5

Chevrel, M.O., Harris, A.J.L., James, M.R., Calabrò, L., Gurioli, L., Pinkerton, H., 2018. The viscosity of pāhoehoe lava: In situ syn-eruptive measurements from Kilauea, Hawaii. Earth Planet. Sci. Lett. 493, 161–171. https://doi.org/10.1016/j.epsl.2018.04.028

Chevrel, M.O., Platz, T., Hauber, E., Baratoux, D., Lavallée, Y., Dingwell, D.B., 2013. Lava flow rheology: A comparison of morphological and petrological methods. Earth Planet. Sci. Lett. 384, 109–120. https://doi.org/10.1016/j.epsl.2013.09.022

Cody, G.D., Mysen, B.O., Lee, S.K., 2005. Structure vs. composition: A solid-state ^{1}H and ^{29}Si NMR study of quenched glasses along the Na_2O-SiO_2-H_2O join. Geochim. Cosmochim. Acta 69, 2373–2384. https://doi.org/10.1016/j.gca.2004.11.012

Costa, A., Caricchi, L., Bagdassarov, N., 2009. A model for the rheology of particle-bearing suspensions and partially molten rocks: Rheology of particle bearing suspensions. Geochem. Geophys. Geosystems 10, Q03010. https://doi.org/10.1029/2008GC002138

Del Gaudio, P., Ventura, G., Taddeucci, J., 2013. The effect of particle size on the rheology of liquid-solid mixtures with application to lava flows: Results from analogue experiments: Rheology of Liquid-Solid Mixtures. Geochem. Geophys. Geosystems 14, 2661–2669. https://doi.org/10.1002/ggge.20172

Di Fiore, F., Vona, A., Costa, A., Mollo, S., Romano, C., 2022. Quantifying the influence of cooling and shear rate on the disequilibrium rheology of a trachybasaltic melt from Mt. Etna. Earth Planet. Sci. Lett. 594, 117725. https://doi.org/10.1016/j.epsl.2022.117725

Di Genova, D.D., Caracciolo, A., Kolzenburg, S., 2018. Measuring the degree of "nanotilization" of volcanic glasses: Understanding syn-eruptive processes recorded in melt inclusions. Lithos 318–319, 209–218. https://doi.org/10.1016/j.lithos.2018.08.011

Di Genova, D.D., Sicola, S., Romano, C., Vona, A., Fanara, S., Spina, L., 2017. Effect of iron and nanolites on Raman spectra of volcanic glasses: A reassessment of existing strategies to estimate the water content. Chem. Geol. 475, 76–86. https://doi.org/10.1016/j.chemgeo.2017.10.035

Di Genova, D., Zandona, A., Deubener, J., 2020. Unravelling the effect of nano-heterogeneity on the viscosity of silicate melts: Implications for glass manufacturing and volcanic eruptions. J. Non-Cryst. Solids 545, 120248. https://doi.org/10.1016/j.jnoncrysol.2020.120248

Dingwell, D.B., 1991. Redox viscometry of some Fe-bearing silicate melts. Am. Mineral. 76, 1560–1562.

Dingwell, D.B., 1986. Viscosity-temperature relationships in the system $Na_2Si_2O_5$-$Na_4Al_2O_5$. Geochim. Cosmochim. Acta 50, 1261–1265. https://doi.org/10.1016/0016-7037(86)90409-6

Dingwell, D.B., Romano, C., Hess, K.-U., 1996. The effect of water on the viscosity of a haplogranitic melt under P-T-X conditions relevant to silicic volcanism. Contrib. Mineral. Petrol. 124, 19–28. https://doi.org/10.1007/s004100050170

Dingwell, D.B., Virgo, D., 1987. The effect of oxidation state on the viscosity of melts in the system Na_2O-FeO-Fe_2O_3-SiO_2. Geochim. Cosmochim. Acta 51, 195–205. https://doi.org/10.1016/0016-7037(87)90231-6

Farquharson, J.I., James, M.R., Tuffen, H., 2015. Examining rhyolite lava flow dynamics through photo-based 3D reconstructions of the 2011–2012 lava flowfield at Cordón-Caulle, Chile. J. Volcanol. Geotherm. Res. 304, 336–348. https://doi.org/10.1016/j.jvolgeores.2015.09.004

Feuillet, N., Jorry, S., Crawford, W.C., Deplus, C., Thinon, I., Jacques, E., Saurel, J.M., Lemoine, A., Paquet, F., Satriano, C., Aiken, C., Foix, O., Kowalski, P., Laurent, A., Rinnert, E., Cathalot, C., Donval, J.-P., Guyader, V., Gaillot, A., Scalabrin, C., Moreira, M., Peltier, A., Beauducel, F., Grandin, R., Ballu, V., Daniel, R., Pelleau, P., Gomez, J., Besançon, S., Geli, L., Bernard, P., Bachelery, P., Fouquet, Y., Bertil, D., Lemarchand, A., Van der Woerd, J., 2021. Birth of a large volcanic edifice offshore Mayotte via lithosphere-scale dyke intrusion. Nat. Geosci. 14, 787-795. https://doi.org/10.1038/s41561-021-00809-x

Feuillet N., 2019. MAYOBS1 cruise, Marion Dufresne R/V. https://doi.org/10.17600/18001217

Fink, J.H., 1983. Structure and emplacement of a rhyolitic obsidian flow: Little Glass Mountain, Medicine Lake Highland, northern California. Geol. Soc. Am. Bull. 94, 362-380. https://doi.org/10.1130/0016-7606(1983)94<362:SAEOAR>2.0.CO;2

Fouquet Y., Feuillet N., 2019. MAYOBS4 cruise, Marion Dufresne R/V. https://doi.org/10.17600/18001238

Fulcher, G.S., 1925. Analysis of recent measurements of the viscosity of glasses. J. Am. Ceram. Soc. 8, 339–355. https://doi.org/10.1111/j.1151-2916.1925.tb16731.x

Gardner, J.E., Thomas, R.M.E., Jaupart, C., Tait, S., 1996. Fragmentation of magma during Plinian volcanic eruptions. Bull. Volcanol. 58, 144–162. https://doi.org/10.1007/s004450050132

Ghiorso, M.S., Sack, R.O., 1995. Chemical mass transfer in magmatic processes IV. A revised and internally consistent thermodynamic model for the interpolation and extrapolation of liquid-solid equilibria in magmatic systems at elevated temperatures and pressures. Contrib. Mineral. Petrol. 119, 197–212. https://doi.org/10.1007/BF00307281

Giordano, D., Ardia, P., Romano, C., Dingwell, D.B., Di Muro, A., Schmidt, M.W., Mangiacapra, A., Hess, K.-U., 2009. The rheological evolution of alkaline Vesuvius magmas and comparison with alkaline series from the Phlegrean Fields, Etna, Stromboli and Teide. Geochim. Cosmochim. Acta 73, 6613–6630. https://doi.org/10.1016/j.gca.2009.07.033

Giordano, D., Dingwell, D.B., 2003. Viscosity of hydrous Etna basalt: implications for Plinian-style basaltic eruptions. Bull. Volcanol. 65, 8–14. https://doi.org/10.1007/s00445-002-0233-2

Giordano, D., Dingwell, D.B., Romano, C., 2000. Viscosity of a Teide phonolite in the welding interval. J. Volcanol. Geotherm. Res. 103, 239–245. https://doi.org/10.1016/S0377-0273(00)00226-2

Giordano, D., Nichols, A.R.L., Dingwell, D.B., 2005. Glass transition temperatures of natural hydrous melts: a relationship with shear viscosity and implications for the welding process. J. Volcanol. Geotherm. Res. 142, 105–118. https://doi.org/10.1016/j.jvolgeores.2004.10.015

Giordano, D., Russell, J.K., Dingwell, D.B., 2008. Viscosity of magmatic liquids: A model. Earth Planet. Sci. Lett. 271, 123–134. https://doi.org/10.1016/j.epsl.2008.03.038

Gonnermann, H.M., 2015. Magma Fragmentation. Annu. Rev. Earth Planet. Sci. 43, 431–458. https://doi.org/10.1146/annurev-earth-060614-105206

Gonnermann, H.M., Houghton, B.F., Adams, N.K., Hildreth, E.W., 2011. The effect of CO_2 on magma vesiculation during explosive volcanic eruptions, in: AGU Fall Meeting Abstracts. pp. V23H-06.

Gurioli, L., Komorowski, J.-C., Berthod, C., Médard, E., Lacombe, T., Verdurme, P., Bachèlery, P., Mitra, S., Falvard, S., Paris, R., Voyer, E., Di Muro, A., Besson, P., Lebas, E., Paquet, F., Cathalot, C., Bermell-Fleury, S., Scalabrin, C., Rinnert, E., Feuillet, N., Thinon, I., and the REVOSIMA consortium, 2023. Anatomy of a submarine past volcanic explosion east Mayotte: quantification of primary fragmentation. IAVCEI Scientific Assembly, Rotorua, New-Zealand.

Harris, A.J.L., Allen, J.S., 2008. One-, two- and three-phase viscosity treatments for basaltic lava flows. J. Geophys. Res. 113, B09212. https://doi.org/10.1029/2007JB005035

Hehlen, B., Courtens, E., Yamanaka, A., Inoue, K., 2002. Nature of the Boson peak of silica glasses from hyper-Raman scattering. J. Non-Cryst. Solids 307, 87–91.

Hui, H., Zhang, Y., 2007. Toward a general viscosity equation for natural anhydrous and hydrous silicate melts. Geochim. Cosmochim. Acta 71, 403–416. https://doi.org/10.1016/j.gca.2006.09.003

Jones, T.J., Reynolds, C.D., Boothroyd, S.C., 2019. Fluid dynamic induced break-up during volcanic eruptions. Nat. Commun. 10, 3828. https://doi.org/10.1038/s41467-019-11750-4

Jorry S., 2019. MAYOBS2 cruise, Marion Dufresne R/V. https://doi.org/10.17600/18001222

Kolzenburg, S., Chevrel, M.O., Dingwell, D.B., 2022. Magma / Suspension Rheology. Rev. Mineral. Geochem. 87, 639–720. https://doi.org/10.2138/rmg.2022.87.14

Kolzenburg, S., Giordano, D., Hess, K.U., Dingwell, D.B., 2018. Shear Rate-Dependent Disequilibrium Rheology and Dynamics of Basalt Solidification. Geophys. Res. Lett. 45, 6466–6475. https://doi.org/10.1029/2018GL077799

Komorowski, J.-C., Gurioli, L., Berthod, C., Médard, E., Verdurme, P., Puzenat, V., Bachèlery, P., Chevrel, O., Paquet, F., Lebas, E., Rinnert, E., Feuillet, N., Fouquet, Y., Thinon, I., Cathalot, C., Jorry, S., Besson, P., Le Friant, A., Di Muro, A.,

Lacombe, T., Deplus, C., Scalabrin, C., Lemoine, A., Pierre, D., Loubrieu, B., Ferrand, P., Bermell-Fleury, S., Pitel-Roudaut, M., Gaillot, A., Jouet, G., Lavayssière, A., Retailleau, L., Foix, O., Jacques, E., Mastin, M., Escartin, J., Hidalgo, S., Nowak, S., Burckel, P., Le Losq, C., Augustin, J.-M., Lemarchand, A., Saurel, J.-M., Peltier, A., Mucig, C., and the REVOSIMA consortium, 2023. The submarine monogenetic volcanic field East of Mayotte (France, Indian Ocean): an exceptional diversity of effusive and explosive processes revealed by recurrent multidisciplinary oceanographic campaigns between 2019 and 2022. IAVCEI Scientific Assembly, Rotorua, New-Zealand.

Le Losq, C., Cicconi, M.R., Neuville, D.R., 2021a. Iron in Silicate Glasses and Melts: Implications for Volcanological Processes, in: Moretti, R., Neuville, D.R. (Eds.), Geophysical Monograph Series. Wiley, pp. 233–253. https://doi.org/10.1002/9781119473206.ch12

Le Losq, C., Mysen, B.O., Cody, G.D., 2015a. Water and magmas: insights about the water solution mechanisms in alkali silicate melts from infrared, Raman, and ^{29}Si solid-state NMR spectroscopies. Prog. Earth Planet. Sci. 2, 22. https://doi.org/10.1186/s40645-015-0052-7Le Losq, C., Neuville, D.R., 2017. Molecular structure, configurational entropy and viscosity of silicate melts: Link through the Adam and Gibbs theory of viscous flow. J. Non-Cryst. Solids 463, 175–188. https://doi.org/10.1016/j.jnoncrysol.2017.02.010

Le Losq, C., Neuville, D.R., 2013. Effect of the Na/K mixing on the structure and the rheology of tectosilicate silica-rich melts. Chem. Geol. 346, 57–71. https://doi.org/10.1016/j.chemgeo.2012.09.009

Le Losq, C., Neuville, D.R., Florian, P., Henderson, G.S., Massiot, D., 2014. The role of Al^{3+} on rheology and structural changes in sodium silicate and aluminosilicate glasses and melts. Geochim. Cosmochim. Acta 126, 495–517. https://doi.org/10.1016/j.gca.2013.11.010

Le Losq, C., Neuville, D.R., Moretti, R., Kyle, P.R., Oppenheimer, C., 2015b. Rheology of phonolitic magmas—the case of the Erebus lava lake. Earth Planet. Sci. Lett. 411, 53–61. https://doi.org/10.1016/j.epsl.2014.11.042

Le Losq, C., Valentine, A.P., Mysen, B.O., Neuville, D.R., 2021b. Structure and properties of alkali aluminosilicate glasses and melts: Insights from deep learning. Geochim. Cosmochim. Acta 314, 27–54. https://doi.org/10.1016/j.gca.2021.08.023

Le Losq, C.L., 2018. Rampy: a Python library for processing spectroscopic (IR, Raman, XAS...) data. https://doi.org/10.5281/ZENODO.1168729

Lejeune, A.M., Bottinga, Y., Trull, T.W., Richet, P., 1999. Rheology of bubble-bearing magmas. Earth Planet. Sci. Lett. 166, 71–84. https://doi.org/10.1016/S0012-821X(98)00278-7

Lejeune, A.-M., Richet, P., 1995. Rheology of crystal-bearing silicate melts: An experimental study at high viscosities. J. Geophys. Res. Solid Earth 100, 4215–4229. https://doi.org/10.1029/94JB02985

Lemoine, A., Briole, P., Bertil, D., Roullé, A., Foumelis, M., Thinon, I., Raucoules, D., de Michele, M., Valty, P., Hoste Colomer, R., 2020. The 2018–2019 seismo-volcanic crisis east of Mayotte, Comoros islands: seismicity and ground deformation markers of an exceptional submarine eruption. Geophys. J. Int. 223, 22–44. https://doi.org/10.1093/gji/ggaa273

Liebske, C., Behrens, H., Holtz, F., Lange, R.A., 2003. The influence of pressure and composition on the viscosity of andesitic melts. Geochim. Cosmochim. Acta 67, 473–485. https://doi.org/10.1016/S0016-7037(02)01139-0

Llewellin, E.W., Manga, M., 2005. Bubble suspension rheology and implications for conduit flow. J. Volcanol. Geotherm. Res. 143, 205–217. https://doi.org/10.1016/j.jvolgeores.2004.09.018

Ma, S., Zhang, X., Morrow, N.R., 1999. Influence of Fluid Viscosity On Mass Transfer Between Rock Matrix And Fractures. J. Can. Pet. Technol. 38. https://doi.org/10.2118/99-07-02

Mader, H.M., Llewellin, E.W., Mueller, S.P., 2013. The rheology of two-phase magmas: A review and analysis. J. Volcanol. Geotherm. Res. 257, 135–158. https://doi.org/10.1016/j.jvolgeores.2013.02.014

Malinovsky, V.K., Sokolov, A.P., 1986. The nature of boson peak in Raman scattering in glasses. Solid State Commun. 57, 757–761. https://doi.org/10.1016/0038-1098(86)90854-9

McClinton, J.T., White, S.M., Colman, A., Rubin, K.H., Sinton, J.M., 2014. The role of crystallinity and viscosity in the formation of submarine lava flow morphology. Bull. Volcanol. 76, 854. https://doi.org/10.1007/s00445-014-0854-2

McMillan, P., 1984. Structural studies of silicate glasses and melts—applications and limitations of Raman spectroscopy. Am. Mineral. 69, 622–644.

Moitra, P., Gonnermann, H.M., Houghton, B.F., Tiwary, C.S., 2018. Fragmentation and Plinian eruption of crystallizing basaltic magma. Earth Planet. Sci. Lett. 500, 97–104. https://doi.org/10.1016/j.epsl.2018.08.003

Moretti, R., 2005. Polymerisation, basicity, oxidation state and their role in ionic modelling of silicate melts. Annals of Geophysics 48. https://doi.org/10.4401/ag-3221

Moretti, R., Le Losq, C., Neuville, D.R., 2014. The amphoteric behavior of water in silicate melts from the point of view of their ionic-polymeric constitution. Chem. Geol. 367, 23–33. https://doi.org/10.1016/j.chemgeo.2013.12.012

Morrison, A., Whittington, A., Smets, B., Kervyn, M., Sehlke, A., 2020. The rheology of crystallizing basaltic lavas from Nyiragongo and Nyamuragira volcanoes, D.R.C. Volcanica 3, 1–28. https://doi.org/10.30909/vol.03.01.0128

Myers, M.L., Druitt, T.H., Schiavi, F., Gurioli, L., Flaherty, T., 2021. Evolution of magma decompression and discharge during a Plinian event (Late Bronze-Age eruption,

Santorini) from multiple eruption-intensity proxies. Bull. Volcanol. 83, 18. https://doi.org/10.1007/s00445-021-01438-3

Mysen, B., 1995. Experimental, in situ, high-temperature studies of properties and structure of silicate melts relevant to magmatic processes. Eur. J. Mineral. 7, 745–766. https://doi.org/10.1127/ejm/7/4/0745

Mysen, B., Richet, P., 2005. Silicate Glasses and Melts, Elsevier. ed, Developments in Geochemistry. Amsterdam, Netherlands.

Mysen, B.O., Cody, G.D., 2005. Solution mechanisms of H_2O in depolymerized peralkaline melts. Geochim. Cosmochim. Acta 69, 5557–5566. https://doi.org/10.1016/j.gca.2005.07.020

Mysen, B.O., Richet, P., 2019. Silicate Glasses and Melts. Elsevier. https://doi.org/10.1016/C2018-0-00864-6

Mysen, B.O., Richet, P., 2005. Silicate glasses and melts: properties and structure, 1st ed. Developments in geochemistry. Elsevier, Amsterdam ; Boston.

Mysen, B.O., Virgo, D., Scarfe, C.M., 1980. Relations between the anionic structure and viscosity of silicate melts—a Raman spectroscopic study. Am. Mineral. 65, 690–710.

Mysen, B.O., Virgo, D., Scarfe, C.M., Cronin, D.J., 1985. Viscosity and structure of iron- and aluminum-bearing calcium silicate melts at 1 atm. Am. Mineral. 70, 487–498.

Mysen, B.O., Virgo, D., Seifert, F.A., 1982. The structure of silicate melts: Implications for chemical and physical properties of natural magma. Rev. Geophys. 20, 353. https://doi.org/10.1029/RG020i003p00353

Nascimento, M.L.F., Aparicio, C., 2007. Data classification with the Vogel–Fulcher–Tammann–Hesse viscosity equation using correspondence analysis. Phys. B Condens. Matter 398, 71–77. https://doi.org/10.1016/j.physb.2007.04.074

Neuville, D.R., 2006. Viscosity, structure and mixing in (Ca, Na) silicate melts. Chem. Geol. 229, 28–41. https://doi.org/10.1016/j.chemgeo.2006.01.008

Neuville, D.R., Richet, P., 1991. Viscosity and mixing in molten (Ca, Mg) pyroxenes and garnets. Geochim. Cosmochim. Acta 55, 1011–1019. https://doi.org/10.1016/0016-7037(91)90159-3

Papale, P., 1999. Strain-induced magma fragmentation in explosive eruptions. Nature 397, 425–428. https://doi.org/10.1038/17109

Pelleter, A.-A., Caroff, M., Cordier, C., Bachelery, P., Nehlig, P., Debeuf, D., Arnaud, N., 2014. Melilite-bearing lavas in Mayotte (France): An insight into the mantle source below the Comores. Lithos 208–209, 281–297. https://doi.org/10.1016/j.lithos.2014.09.012

Pistolesi, M., Rosi, M., Cioni, R., Cashman, K.V., Rossotti, A., Aguilera, E., 2011. Physical volcanology of the post-twelfth-century activity at Cotopaxi volcano, Ecuador:

Behavior of an andesitic central volcano. Geol. Soc. Am. Bull. 123, 1193–1215. https://doi.org/10.1130/B30301.1

Poole, J.P., 1949. Low-temperature viscosity of alkali silicate glasses. J. Am. Ceram. Soc. 32, 230–233. https://doi.org/10.1111/j.1151-2916.1949.tb18952.x

Popa, R.-G., Bachmann, O., Huber, C., 2021. Explosive or effusive style of volcanic eruption determined by magma storage conditions. Nat. Geosci. 14, 781–786. https://doi.org/10.1038/s41561-021-00827-9

Prival, J.-M., Harris, A.J.L., Zanella, E., Robustelli Test, C., Gurioli, L., Chevrel, O., Biren, J., 2022. Emplacement dynamics of a crystal-rich, highly viscous trachytic flow of the Sancy stratovolcano, France. GSA Bull. https://doi.org/10.1130/B36415.1

Puzenat V., Feuillet N., Komorowski J.-C., Escartin J., Deplus C., Bachèlery P., Berthod C., Gurioli L., Scalabrin C., Cathalot C., Rinnert, E., Loubrieu, B., Pierre, D., Pitel-Roudaut, M., Tanguy, N., Fouquet, Y., Jorry, S., Lebas, E., Paquet, F., and Thinon, I., 2023. Volcano-tectonic structures of Mayotte's upper submarine slope: insights from high-resolution bathymetry and in-situ imagery from a deep towed camera. **Accepted to Comptes Rendus Geoscience, Special issue.**

Ramírez-Uribe, I., Siebe, C., Chevrel, M.O., Ferres, D., Salinas, S., 2022. The late Holocene Nealtican lava-flow field, Popocatépetl volcano, central Mexico: Emplacement dynamics and future hazards. GSA Bull. 134, 2745–2766. https://doi.org/10.1130/B36173.1

REVOSIMA, 2022. Campagne MD239-MAYOBS23 : Note finale. Vendredi 23 Juillet 2022 https://www.ipgp.fr/sites/default/files/md239-mayobs23_note-finale_20220727.pdf

Richet, P., 1984. Viscosity and configurational entropy of silicate melts. Geochim. Cosmochim. Acta 48, 471–483. https://doi.org/10.1016/0016-7037(84)90275-8

Rinnert E., Lebas E., Jorry S., Feuillet N., Thinon I., Fouquet Y., 2019. MAYOBS, https://doi.org/10.18142/291

Rinnert, E., Thinon, I., Feuillet, N., 2020. MD 228 / MAYOBS15 cruise, Marion Dufresne R/V. https://doi.org/10.17600/18001745

Rinnert, E., Thinon, I., Lebas, E., 2021. MAYOBS21 cruise, Marion Dufresne R/V. https://doi.org/10.17600/18001986

Rinnert, E., Cathalot, C., Feuillet, N., 2021. Géoflamme cruise, Pourquoi pas ? R/V. https://doi.org/10.17600/18001297

Robert, G., Smith, R.A., Whittington, A.G., 2019. Viscosity of melts in the $NaAlSiO_4$-$KAlSiO_4$-SiO_2 system: Configurational entropy modelling. J. Non-Cryst. Solids 524, 119635. https://doi.org/10.1016/j.jnoncrysol.2019.119635

Romano, C., Giordano, D., Papale, P., Mincione, V., Dingwell, D.B., Rosi, M., 2003. The dry and hydrous viscosities of alkaline melts from Vesuvius and Phlegrean Fields. Chem. Geol. 202, 23-38. https://doi.org/10.1016/S0009-2541(03)00208-0

Scarfe, C., Mysen, B.O., Virog, D., 1987. Pressure dependence of the viscosity of silicate melts. Magmat. Process. Physicochem. Princip 59–67.

Scheu, B., Dingwell, D.B., 2022. Magma Fragmentation. Rev. Mineral. Geochem. 87, 767–800. https://doi.org/10.2138/rmg.2021.87.16

Schiavi, F., Bolfan-Casanova, N., Withers, A.C., Médard, E., Laumonier, M., Laporte, D., Flaherty, T., Gómez-Ulla, A., 2018. Water quantification in silicate glasses by Raman spectroscopy: Correcting for the effects of confocality, density and ferric iron. Chem. Geol. 483, 312–331. https://doi.org/10.1016/j.chemgeo.2018.02.036

Shaw, H.R., 1972. Viscosities of magmatic silicate liquids; an empirical method of prediction. Am. J. Sci. 272, 870–893. https://doi.org/10.2475/ajs.272.9.870

SHOM, 2016. MNT bathymetrique de la façade de Mayotte (Projet Homonim).http://dx.doi.org/10.17183/MNT_MAYOTTE_100m_HOMONIM_WGS84

Spera, F.J., Borgia, A., Strimple, J., Feigenson, M., 1988. Rheology of melts and magmatic suspensions: 1. Design and calibration of concentric cylinder viscometer with application to rhyolitic magma. J. Geophys. Res. Solid Earth 93, 10273–10294. https://doi.org/10.1029/JB093iB09p10273

Starodub, K., Wu, G., Yazhenskikh, E., Müller, M., Khvan, A., Kondratiev, A., 2019. An Avramov-based viscosity model for the SiO_2-Al_2O_3-Na_2O-K_2O system in a wide temperature range. Ceram. Int. 45, 12169–12181. https://doi.org/10.1016/j.ceramint.2019.03.121

Stebbins, J.F., Farnan, I., Xue, X., 1992. The structure and dynamics of alkali silicate liquids: A view from NMR spectroscopy. Chem. Geol. 96, 371–385. https://doi.org/10.1016/0009-2541(92)90066-E

Stebbins, J.F., Xu, Z., 1997. NMR evidence for excess non-bridging oxygen in an aluminosilicate glass. Nature 390, 60–62. https://doi.org/10.1038/36312

Takahashi, Y., Osada, M., Masai, H., Fujiwara, T., 2009. Crystallization and nanometric heterogeneity in glass: *In situ* observation of the boson peak during crystallization. Phys. Rev. B 79, 214204. https://doi.org/10.1103/PhysRevB.79.214204

Tammann, G., Hesse, W., 1926. Die Abhängigkeit der Viscosität von der Temperatur bie unterkühlten Flüssigkeiten. Z. Für Anorg. Allg. Chem. 156, 245–257. https://doi.org/10.1002/zaac.19261560121

Thivet, S., Hess, K.-U., Dingwell, D. B., Gurioli, L., Di Muro, A., Berthod, C., Lacombe, T., Komorowski, J.-C., 2023. Volatile distributions and contents in recent volcanic products from Mayotte active volcanic chain revealed by simultaneous thermal (STA) and evolved gas analyses (EGA-MS). **Submitted to Chem. Geol. - *CHEMGE-S-22-00968***

Thomas, N., Jaupart, C., Vergniolle, S., 1994. On the vesicularity of pumice. J. Geophys. Res. 99, 15633. https://doi.org/10.1029/94JB00650

Vetere, F., Murri, M., Alvaro, M., Domeneghetti, M.C., Rossi, S., Pisello, A., Perugini, D., Holtz, F., 2019. Viscosity of Pyroxenite Melt and Its Evolution During Cooling. J. Geophys. Res. Planets. 124, 1541-1469. https://doi.org/10.1029/2018JE005851

Vogel, D.H., 1921. Das Temperaturabhaengigkeitsgesetz der Viskositaet von Fluessigkeiten. Physikalische Zeitschrift 22, 645.

Wadsworth, F.B., Witcher, T., Vossen, C.E.J., Hess, K.-U., Unwin, H.E., Scheu, B., Castro, J.M., Dingwell, D.B., 2018. Combined effusive-explosive silicic volcanism straddles the multiphase viscous-to-brittle transition. Nat. Commun. 9, 4696. https://doi.org/10.1038/s41467-018-07187-w

Whittington, A., Richet, P., Holtz, F., 2000. Water and the viscosity of depolymerized aluminosilicate melts. Geochim. Cosmochim. Acta 64, 3725–3736. https://doi.org/10.1016/S0016-7037(00)00448-8

Whittington, A., Richet, P., Linard, Y., Holtz, F., 2001. The viscosity of hydrous phonolites and trachytes. Chem. Geol. 174, 209–223. https://doi.org/10.1016/S0009-2541(00)00317-X

Xue, X., Kanzaki, M., 2006. Depolymerization effect of water in aluminosilicate glasses: Direct evidence from ^{1}H-^{27}Al heteronuclear correlation NMR. Am. Mineral. 91, 1922–1926. https://doi.org/10.2138/am.2006.2365

Xue, X., Kanzaki, M., 2004. Dissolution mechanisms of water in depolymerized silicate melts: Constraints from ^{1}H and ^{29}Si NMR spectroscopy and ab initio calculations. Geochim. Cosmochim. Acta 68, 5027–5057. https://doi.org/10.1016/j.gca.2004.08.016

Zhang, Y., Ni, H., 2010. Diffusion of H, C, and O Components in Silicate Melts. Rev. Mineral. Geochem. 72, 171–225. https://doi.org/10.2138/rmg.2010.72.5

Declaration of interests

☒The authors declare that they have no known competing financial interests or personal relationships that could have appeared to influence the work reported in this paper.

☐The authors declare the following financial interests/personal relationships which may be considered as potential competing interests:

- Pure liquid viscosity measurements are performed on submarine melts from the basanite - phonolite trend .

- At super-liquidus temperatures, viscosity ($\log_{10}$ Pas) is comprised between 0.11 to 1.16 for basanite, 0.89 - 1.97 for tephri-phonolite and 1.75 to 3.89 phonolites.

- A discrepancy is revealed by comparing experimental measurements and parametric viscosity models.

- The effect of water at the eruptive temperatures for such compositions is explored.